NMR Studies of Coupled Low- and High-Barrier Hydrogen Bonds in Pyridoxal-5'-phosphate Model Systems in Polar Solution

ARTICLE *in* JOURNAL OF THE AMERICAN CHEMICAL SOCIETY · JUNE 2007

Impact Factor: 12.11 · DOI: 10.1021/ja070296+ · Source: PubMed

4 AUTHORS, INCLUDING:

Michael D Toney
University of California, Davis
99 PUBLICATIONS **3,542** CITATIONS
SEE PROFILE

Hans-Heinrich Limbach
Freie Universität Berlin
333 PUBLICATIONS **9,021** CITATIONS
SEE PROFILE

J|A|C|S
ARTICLES
Published on Web 04/25/2007

NMR Studies of Coupled Low- and High-Barrier Hydrogen Bonds in Pyridoxal-5′-phosphate Model Systems in Polar Solution

Shasad Sharif,[†] Gleb S. Denisov,[‡] Michael D. Toney,[§] and Hans-Heinrich Limbach*,[†]

Contribution from the Institut für Chemie und Biochemie, Takustrasse 3, Freie Universität Berlin, D-14195 Berlin, Germany, the Institute of Physics, St. Petersburg State University, 198504 St. Petersburg, Russian Federation, and the Department of Chemistry, University of California-Davis, Davis, California, 95616

Received January 15, 2007; E-mail: limbach@chemie.fu-berlin.de

Abstract: The ^{1}H and ^{15}N NMR spectra of several ^{15}N-labeled pyridoxal-5′-phosphate model systems have been measured at low temperature in various aprotic and protic solvents of different polarity, i.e., dichloromethane-d_2, acetonitrile-d_3, tetrahydrofuran-d_8, freon mixture $CDF_3/CDClF_2$, and methanol. In particular, the ^{15}N-labeled 5′-triisopropyl-silyl ether of *N*-(pyridoxylidene)-tolylamine (**1a**), *N*-(pyridoxylidene)-methylamine (**2a**), and the Schiff base with ^{15}*N*-2-methylaspartic acid (**3a**) and their complexes with proton donors such as triphenylmethanol, phenol, and carboxylic acids of increasing strength were studied. With the use of hydrogen bond correlation techniques, the ^{1}H/^{15}N chemical shift and scalar coupling data could be associated with the geometries of the intermolecular O1H1N1 (pyridine nitrogen) and the intramolecular O2H2N2 (Schiff base) hydrogen bonds. Whereas O1H1N1 is characterized by a series of asymmetric low-barrier hydrogen bonds, the proton in O2H2N2 faces a barrier for proton transfer of medium height. When the substituent on the Schiff base nitrogen is an aromatic ring, the shift of the proton in O1H1N1 from oxygen to nitrogen has little effect on the position of the proton in the O2H2N2 hydrogen bond. By contrast, when the substituent on the Schiff base nitrogen is a methyl group, a proton shift from O to N in O1H1N1 drives the tautomeric equilibrium in O2H2N2 from the neutral O2−H2···N2 to the zwitterionic $O2^{-}\cdots H2-N2^{+}$ form. This coupling is lost in aqueous solution where the intramolecular O2H2N2 hydrogen bond is broken by solute−solvent interactions. However, in methanol, which mimics hydrogen bonds to the Schiff base in the enzyme active site, the coupling is preserved. Therefore, the reactivity of Schiff base intermediates in pyridoxal-5′-phosphate enzymes can likely be tuned to the requirements of the reaction being catalyzed by differential protonation of the pyridine nitrogen.

Introduction

Pyridoxal-5′-phosphate (PLP, vitamin B_6; Scheme 1) is required as a cofactor in a truly remarkable variety of enzyme-catalyzed transformations of amines and amino acids, e.g., transamination, decarboxylation, and racemization.[1−5] According to the crystal structures of various aspartate aminotransferases (AspATs), the cofactor forms Schiff bases or "aldimines" with amino acids.[6−11] In the absence of a substrate, PLP forms an "internal aldimine" with the ϵ-amino group of a lysine residue of the enzyme. When amino acid substrates bind to the active site, an "external" aldimine intermediate is formed, representing the first step of the catalytic cycle (Scheme 1).[1,2] External aldimines can also be formed with modified amino acids such as 2-methylaspartic acid (2-MeAsp), which inhibit the enzyme.[7−10]

The cofactor is embedded in a hydrogen bond network that is essential for the high catalytic activity but whose function in controlling reactivity and reaction specificity is not fully understood. Several hydrogen bonds are formed between various amino acid side chains and the phosphate group of PLP which is present as the dianion (Scheme 1). In order to characterize these hydrogen bonds, aldimine model systems have been designed and studied by liquid-state NMR.[12−17] It appears that

[†] Freie Universität Berlin.
[‡] St. Petersburg State University.
[§] University of California-Davis.

(1) Christen, P.; Metzler, D. E. *Transaminases*; J. Wiley & Sons: New York, 1985; pp 37−101.
(2) Snell, E. E.; Di Mari, S. J. *The Enzymes Vol. 2—Kinetics and Mechanism*, 3rd ed.; Boyer, P.D., Ed.; Academic Press: New York, 1970; pp 335−362.
(3) Spies, M. A.; Toney, M. D. *Biochemistry* **2003**, *42*, 5099−5107.
(4) Malashkevich, V. N.; Toney, M. D.; Jansonius, J. N. *Biochemistry* **1993**, *32*, 13451−13462.
(5) Zhou, X.; Toney, M. D. *Biochemistry* **1999**, *38*, 311−320.
(6) Jansonius, J. N. *Curr. Opin. Struct. Biol.* **1998**, *8*, 759−769.
(7) Stamper, C. G. F.; Morollo, A. A.; Ringe, D. *Biochemistry* **1998**, *37*, 10438−10445.
(8) Rhee, S.; Silva, M. M.; Hyde, C. C.; Rogers, P. H.; Metzler, C. M.; Metzler, D. E.; Arnone, A. *J. Biol. Chem.* **1997**, *272*, 17293−17302.
(9) Jager, J.; Moser, M.; Sauder, U.; Jansonius, J. N. *J. Mol. Biol.* **1994**, *239*, 285−305.
(10) Okamoto, A.; Higuchi, T.; Hirotsu, K.; Kuramitsu, S.; Kagamiyama, H. *J. Biochem.* **1994**, *116*, 95−107.
(11) Smith, D. L.; Almo, S. C.; Toney, M. D.; Ringe, D. *Biochemistry* **1989**, *28*, 8161−8167.
(12) Sharif, S; Chan Huot, M.; Tolstoy, P. M.; Toney, M. D.; Limbach, H. H. *J. Phys. Chem. B* **2007**, *111*, 3869−3876.

Scheme 1. Overview of the First Step of the Catalytic Cycle of Vitamin B_6-Dependent Enzymes[a]

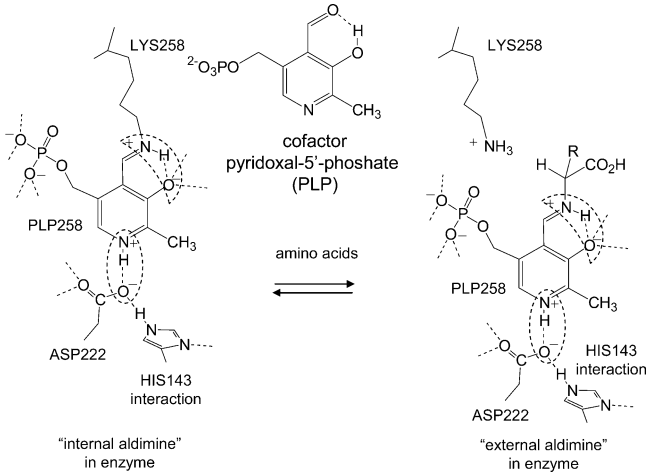

[a] Shown is the cofactor pyridoxal-5′-phosphate (PLP) formation to the external aldimine from the internal aldimine in the enzyme.

the phosphate group acts as an electron donor, increasing the basicity of the cofactor.[12] The phenolic oxygen forms a number of OHO hydrogen bonds to neighboring proton-donating side chains (Scheme 1).

In many PLP-dependent enzymes, the pyridine ring of the cofactor is involved in an intermolecular OHN hydrogen bond with the carboxylate group of the aspartate side chain, which is itself hydrogen bonded to other residues (Scheme 1).[18−23] For these enzymes, it is believed that the pyridine ring nitrogen is protonated and the aspartic acid side chain is ionized.[1,2] However, recent liquid and solid-state NMR experiments of complexes of pyridine derivatives with carboxylic acids have shown that there are not just two extreme protonation states of the pyridine ring (i.e., unprotonated and protonated), rather a continuous spectrum of protonation states. Here, an increase of the acidity of the donor and of the solvent polarity causes a continuous shift of the proton from oxygen to nitrogen, i.e., from O−H···N via $O^{\delta-}\cdot\cdot H\cdot\cdot N^{\delta+}$ to $O^{-}\cdot\cdot\cdot H-N^{+}$, where $O^{\delta-}\cdot\cdot H\cdot\cdot N^{\delta+}$ exhibits the shortest distance O···N.[24−33]

Scheme 2. Schematic View of the Keto−Enol Tautomerism (a) of the Schiff Bases; (b) Influence of the Solvent Polarity and Hydrogen Bond Formation of Proton Donors; (c) Aldimine Models That Mimic the Coupling of the Inter- and Intramolecular Hydrogen Bonds; (d) Schiff Bases That Mimic the Phosphor Group Interaction in Aqueous Solution

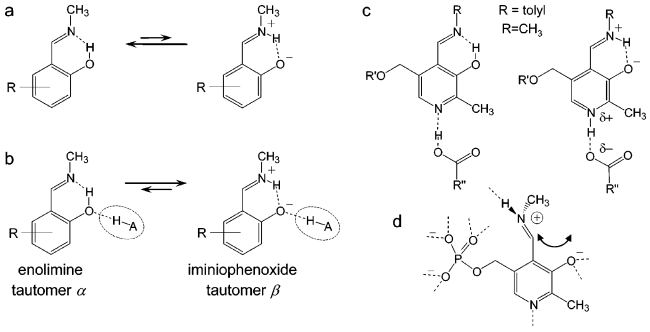

Especially under debate is the intramolecular OHN hydrogen bond between the phenolic oxygen and the imino nitrogen of the cofactor. Model studies have shown that aldimines exhibit a keto−enol tautomerism between a neutral enolimine form and a zwitterionic iminiophenoxide form as illustrated schematically in Scheme 2a, which interconvert very rapidly via proton transfer.[34−39] It has been argued that the positive charge on the imino nitrogen is a prerequisite for catalytic activity and that during the catalytic mechanism the proton shifts between the imino nitrogen and phenolic oxygen.[1,2] Recently, it was shown by NMR that either an increase of the solvent polarity or hydrogen bond formation to proton donors (or both) stabilize the iminiophenoxide form (Scheme 2b), which may be the reason for the above-mentioned OHO hydrogen bonds to the phenolic oxygen in enzyme active sites.[40]

The question of whether the inter- and intramolecular OHN hydrogen bonds are coupled has been studied recently by X-ray crystallography[41] and by solid-state NMR[42] of Schiff base−carboxylic acid model complexes depicted in Scheme 2c. In the case of the Schiff base with 4-methylaniline, proton shifts

(13) Schnackerz, K. D.; Keller, J.; Phillips, R. S.; Toney, M. D. *Biochim. Biophys. Acta* **2006**, *1764*, 230−238.
(14) Schnackerz, K. D.; Wahler, G.; Vincent, M. G.; Jansonius, J. N. *Eur. J. Biochem.* **1989**, *185*, 525−531.
(15) Schnackerz, K. D. *Biochim. Biophys. Acta* **1984**, *789*, 241−244.
(16) Mattingly, M. E.; Mattingly, J. R., Jr.; Martinez-Carrion, M. *J. Biol. Chem.* **1982**, *257*, 8872−8878.
(17) Martinez-Carrion, M. *Eur. J. Biochem.* **1975**, *54*, 39−43.
(18) Mollova, E. T.; Metzler, D. E.; Kintanar, A.; Kagamiyama, H.; Hayashi, H.; Hirotsu, K.; Miyahara, I. *Biochemistry* **1997**, *36*, 615−625.
(19) Metzler, D. E.; Metzler, C. M.; Scott, R. D.; Mollova, E. T.; Kagamiyama, H.; Yano, T.; Kuramitsu, S.; Hayashi, H.; Hirotsu, K.; Miyahara, I. *J. Biol. Chem.* **1994**, *269*, 28027−28033.
(20) Metzler, D. E.; Metzler, C. M.; Mollova, E. T.; Scott, R. D.; Tanase, S.; Kogo, K.; Higaki, T.; Morino, Y. *J. Biol. Chem.* **1994**, *269*, 28017−28026.
(21) Metzler, C. M.; Metzler, D. E.; Kintanar, A.; Scott, R. D.; Marceau, M. *Biochem. Biophys. Res. Commun.* **1991**, *178*, 385−392.
(22) Kintanar, A.; Metzler, C. M.; Metzler, D. E.; Scott, R. D. *J. Biol. Chem.* **1991**, *266*, 17222−17229.
(23) Yano, T.; Kuramitsu, S.; Tanase, S.; Morino, Y.; Hiromi, K.; Kagamiyama, H. *J. Biol. Chem.* **1991**, *266*, 6079−6085.
(24) Limbach, H. H.; Pietrzak, M.; Sharif, S.; Tolstoy, P. M.; Shenderovich, I. G.; Smirnov, S. N.; Golubev, N. S.; Denisov, G. S. *Chem. Eur. J.* **2004**, *10*, 5195−5204.
(25) Limbach, H. H.; Pietrzak, M.; Benedict, H.; Tolstoy, P. M.; Golubev, N. S.; Denisov, G. S. *J. Mol. Struct.* **2004**, *706*, 115−119.
(26) Shenderovich, I. G.; Tolstoy, P. M.; Golubev, N. S.; Smirnov, S. N.; Denisov, G. S.; Limbach, H. H. *J. Am. Chem. Soc.* **2003**, *125*, 11710−11720.
(27) Shenderovich, I. G.; Buntkowsky, G.; Schreiber, A.; Gedat, E.; Sharif, S.; Albrecht, J.; Golubev, N. S.; Findenegg, G. H.; Limbach, H. H. *J. Phys. Chem. B* **2003**, *107*, 11924−11939.
(28) Lorente, P.; Shenderovich, I. G.; Golubev, N. S.; Denisov, G. S.; Buntkowsky, G.; Limbach, H. H. *Magn. Reson. Chem.* **2001**, *39*, S18−S29.
(29) Smirnov, S. N.; Benedict, H.; Golubev, N. S.; Denisov, G. S.; Kreevoy, M. M.; Schowen, R. L.; Limbach, H. H. *Can. J. Chem.* **1999**, *77*, 943−949.
(30) Tolstoy, P. M.; Smirnov, S. N.; Shenderovich, I. G.; Golubev, N. S.; Denisov, G. S.; Limbach, H. H. *J. Mol. Struct.* **2004**, *700*, 19−27.
(31) Golubev, N. S.; Shenderovich, I. G.; Smirnov, S. N.; Denisov, G. S.; Limbach, H. H. *Chem. Eur. J.* **1999**, *5*, 492−497.
(32) Golubev, N. S.; Denisov, G. S.; Smirnov, S. N.; Shchepkin, D. N.; Limbach, H. H. *Z. Phys. Chem.* **1996**, *196*, 73−84.
(33) Smirnov, S. N.; Golubev, N. S.; Denisov, G. S.; Benedict, H.; Schah-Mohammedi, P.; Limbach, H. H. *J. Am. Chem. Soc.* **1996**, *118*, 4094−4101.
(34) Filarowski, A.; Koll, A.; Rospenk, M.; Krol-Starzomska, I.; Hansen, P. E. *J. Phys. Chem. A* **2005**, *109*, 4464−4473.
(35) Dziembowska, T.; Rozwadowski, Z.; Filarowski, A.; Hansen, P. E. *Magn. Reson. Chem.* **2001**, *39*, S67−S80.
(36) Rozwadowski, Z.; Dziembowska, T. *Magn. Reson. Chem.* **1999**, *37*, 274−278.
(37) Rozwadowski, Z.; Majewski, E.; Dziembowska, T.; Hansen, P. E. *J. Chem. Soc., Perkin Trans. 2* **1999**, 2809−2817.
(38) Benedict, C.; Langer, U.; Limbach, H. H.; Ogata, H.; Takeda, S. *Ber. Bunsen-Ges. Phys. Chem.* **1998**, *102*, 335−339.
(39) Hansen, P. E.; Sitkowski, J.; Stefaniak, L.; Rozwadowski, Z.; Dziembowska, T. *Ber. Bunsen-Ges. Phys. Chem.* **1998**, *102*, 410−413.
(40) Sharif, S.; Denisov, G. S.; Toney, M. D.; Limbach, H. H. *J. Am. Chem. Soc.* **2006**, *128*, 3375−3387.
(41) Sharif, S.; Powell, D. R.; Schagen, D.; Steiner, T.; Toney, M. D.; Fogle, E.; Limbach, H. H. *Acta Crystallogr., Sect. B* **2006**, *B62*, 480−487.
(42) Sharif, S.; Schagen, D.; Toney, M. D.; Limbach, H. H. *J. Am. Chem. Soc.* **2007**, *129*, 4440−4455.

Scheme 3. Schiff Base−Carboxylic Acid Complexes and the Effect of Microsolvation by Alcohol on the Inter- and Intramolecular H-Bonds

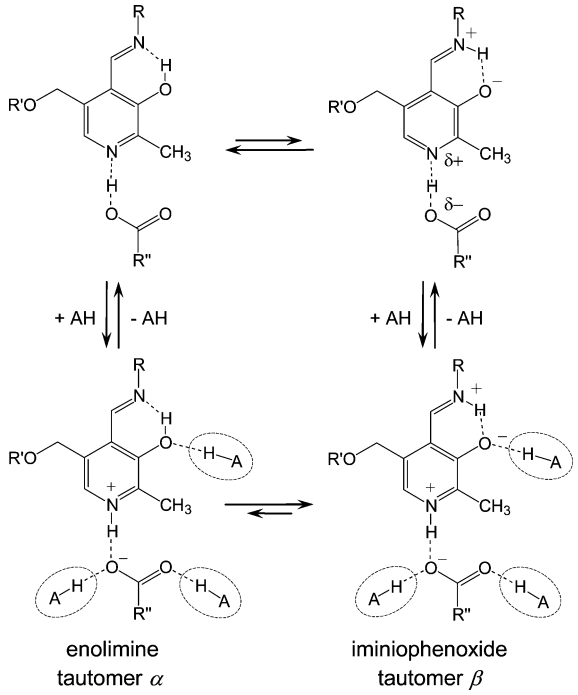

toward the pyridine nitrogen increased the O···H and decreased the H···N distances of the intramolecular OHN hydrogen bond only slightly.[41,42] By contrast, in the case of the Schiff base with methylamine the imino nitrogen is much more basic, and only double-zwitterionic complexes were observed.[41,42] Thus, the details of the coupling of the two H-bonds have not yet been elucidated.

Recently, an interesting observation was made for aldimine models in aqueous solution (Scheme 2d).[12] At pH 7.35 (physiological conditions) the pyridine ring is not protonated and the mutual coupling is suppressed in aqueous solution. This result was associated with a breaking of the intramolecular OHN hydrogen bond by the surrounding water molecules, which is probably assisted by a conformational isomerism about the C−C single bond (Scheme 2d).[12]

In order to understand further the behavior of the cofactor in the enzyme environment, we have, therefore, extended our studies of ^{15}N-labeled cofactor−carboxylic acid hydrogen-bonded model complexes to aprotic polar environments, where low-temperature ^{1}H and ^{15}N NMR spectroscopy were used to obtain hydrogen bond information. In order to mimic the polar but aprotic enzyme environment we used polar solvents such as dichloromethane-d_2, acetonitrile-d_3, tetrahydrofuran-d_8, and in particular, the freon mixture $CDF_3/CDClF_2$ that allows one to perform low-temperature NMR experiments in the regime of slow hydrogen bond exchange.[43,44] The hydrogen bonds formed by the cofactor in the active site environment (other than the two OHN hydrogen bridges) were modeled by added alcohol molecules. We chose methanol as a proton donor, interacting with the model Schiff bases as illustrated schematically in Scheme 3. We find that the microsolvation neither breaks the two OHN hydrogen bonds nor prevents their mutual coupling, but amplifies this coupling to ensure that the imino nitrogen is entirely protonated, as necessary for the catalytic activity.

The structures of all compounds studied are depicted in Scheme 4. We prepared the ^{15}N-labeled Schiff bases of pyridoxal **1** and **2**, containing a tolyl and a methyl group, respectively. Here, the phosphate group was omitted, or replaced by a 5′-triisopropyl-silyl ether protecting group for increased solubility. These compounds as well as some of their complexes with carboxylic acids were part of our previous X-ray[41] and solid-state NMR[42] studies. In addition, we prepared the Schiff base **3** containing the designed ^{15}N-labeled 2-MeAsp, which is known to act as an inhibitor of AspAT.

Finally, we performed *ab initio* calculations in order to determine the detailed molecular structures of some of the compounds studied here. In addition, theoretical analysis of interaction energies provides information about the stability of the adducts studied.

Materials and Methods

Materials. Triphenylmethanol, phenol, acetic acid, formic acid, chloroacetic acid, dichloroacetic acid, trifluoroacetic acid, perfluorobutyric acid, and pyridoxal hydrochloride were purchased from Aldrich. Pyridoxal hydrochloride was neutralized with 1 M $NaHCO_3$ followed by lyophilization. The isotopically enriched compounds acetonitrile-d_3, dichloromethane-d_2, dimethylsulfoxide-d_6 (DMSO), methanol-d_1/-d_3/-d_4, chloroform-d_1, tetrahydrofuran-d_8 (THF), trifluoroacetic acid-d_1 and ammonium chloride $^{15}NH_4Cl$ (98% ^{15}N-enriched) were purchased from Deutero GmbH. The procedures for obtaining the ^{15}N-labeled Schiff bases, 5′-triisopropyl-silyl ether of *N*-(pyridoxylidene)-tolylamine (**1a**) and *N*-(pyridoxylidene)-methylamine (**2a**), were described in ref 42. The synthesis of the Schiff base (**3a**) containing the inhibitor ^{15}N-2-methylaspartic acid (2-MeAsp) is described below.

The deuterated freon gas mixture $CDF_3/CDClF_2$ for the low-temperature NMR experiments, whose composition varied between 1:2 and 1:3, was prepared from chloroform-d_1 by a modified recipe proposed by Siegel and Anet.[45] Details of the synthesis and properties of the freonic mixtures were reported recently.[46]

We prepared ^{15}N-labeled 2-MeAsp from a mixture of the corresponding ketone, ^{15}N-ammonium chloride, and sodium cyanide. The synthesis of ^{15}N-labeled 2-MeAsp was done in analogy to the procedures of isotope labeling of aminoisobutanoic acid: ^{15}N labeling was described by Ogrel[47] et al.; ^{13}C labeling by Zhou[48] et al. A detailed description of the preparation is stated below.

1. Synthesis of ^{15}N-2-Methylaspartic Acid (2-MeAsp). Strecker synthesis using ^{15}N-labeled ammonium chloride was employed. A solution of 2 g (43 mmol) of NaCN and 1.2 g (22 mmol) of 95% ^{15}N-enriched $^{15}NH_4Cl$ in 10 mL of water was made. Then 5 g (5 mL, 43 mmol) of acetoacetic acid methylester in 10 mL of dichloromethane was added dropwise. The reaction mixture was stirred in a sealed ampule for 12 h at room temperature. After that the reaction mixture was hydrolyzed for 2 h with 10 mL concd HCl at 100 °C. The solvent was distilled off, the dry residue was dissolved in methanol, and the solvent was evaporated. The latter procedure was repeated several times. The crude product was dissolved in about 2 mL of deionized water and loaded onto a 2 cm × 30 cm Amberlite IR-120 cation-exchange

(43) Golubev, N. S.; Smirnov, S. N.; Gindin, V. A.; Denisov, G. S.; Benedict, H.; Limbach, H. H. *J. Am. Chem. Soc.* **1994**, *116*, 12055−12056.
(44) Denisov, G. S.; Golubev, N. S. *J. Mol. Struct.* **1981**, *75*, 311−326.
(45) Siegel, J. S.; Anet, F. A. L. *J. Org. Chem.* **1988**, *53*, 2629−2630.
(46) Shenderovich, I. G.; Burtsev, A. P.; Denisov, G. S.; Golubev, N. S.; Limbach, H. H. *Magn. Reson. Chem.* **2001**, *39*, S91−S99.
(47) Ogrel, A.; Rimavi, V.; Raap, J.; Shvets, V. *Russ. J. Org. Chem. (Engl. Transl.)* **2001**, *37*, 475−479; *Zh. Org. Khim.* **2001**, *37*, 510−514.
(48) Zhou, X.; Jin, X.; Medhekar, R.; Chen, X.; Dieckmann, T.; Toney, M. D. *Biochemistry* **2001**, *40*, 1367−1377.

Scheme 4. (a) Aldenamine Schiff Base (**1a**−**1j**) and Its Derivatives Studied in This Work; (b) Aldimine Schiff Base (**2a**−**2d**) and Its Derivatives Studied in This Work, **2d** Is Only Studied Theoretically; (c) Amino Acid Substrate (**3a** and **3b**) and Its Derivatives Studied in This Work

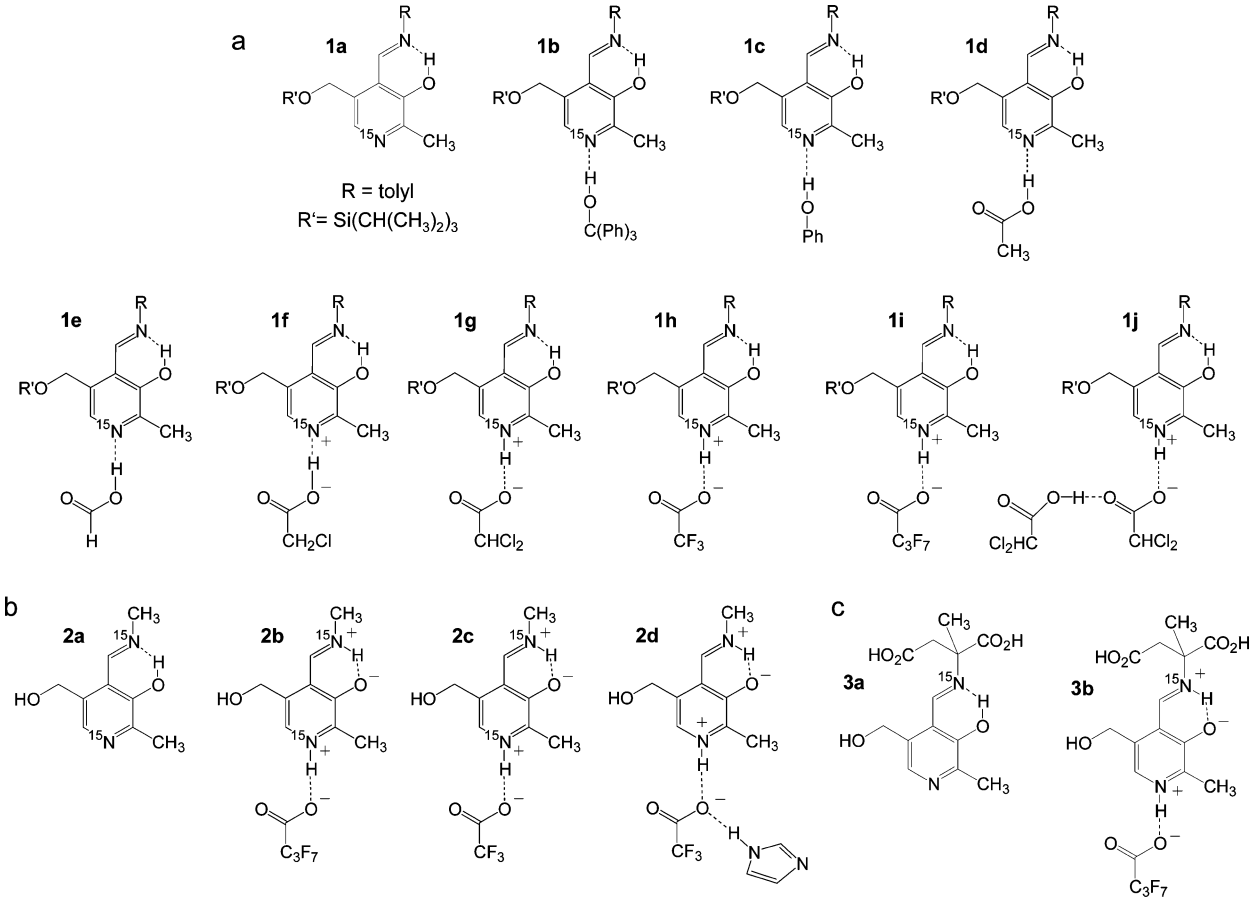

column. The column was washed with deionized water, and the product eluted with 1 M NH_4OH. After evaporating off the solvent the desired product was washed with methanol. An total of 0.8 g of colorless crystals was obtained with a final yield of 24%, based on the starting $^{15}NH_4Cl$. The product shows with ninhydrin (1% in water, heating of the solution gives a blue color change) a positive testing for amino groups. The ^{15}N isotopic enrichment was above 80%, estimated with mass and NMR spectroscopy. Mp 184−186 °C (literature 175−176 °C[49−53]). ^1H NMR (500 MHz, D_2O, RT) δ (ppm/TMS) = 1.62 (d, $^3J(^{15}N,H) = 2.0$ Hz, 3H, $-CH_3$), 2.78 (dd, $^4J(H,H) = 17.5$ Hz, $^3J(^{15}N,H) = 2.0$ Hz, 1H, $-CH'H$), 2.95 (dd, $^4J(H,H) = 17.5$ Hz, $^3J(^{15}N,H) = 3.5$ Hz, 1H, $-CH'H$). The ^{15}N enrichment of 86−95% was estimated from the ratio between the doublet ($^{15}N-H$) and singlet ($^{14}N-H$). ^{13}C {^1H} NMR (125 MHz, DMSO-d_6, RT) δ (ppm/TMS) = 174.7 ($-CH_2-COOH$), 171.8 ($-COOH$), 56.6 ($H_2{}^{15}N-C$, $^1J(^{15}N,^{13}C) = 5.9$ Hz), 42.1 ($-CH_2-$), 23.7 ($-CH_3$). ^{15}N NMR (50.68 MHz, DMSO-d_6, RT) δ (ppm/$^{15}NH_4Cl$) = 5.3 ($H_2{}^{15}N-$). MS FAB$^-$ (H_2O/glycerin): $m/z = 145$ ([M]$^-$, ^{14}N-MeAsp, 14.29%), 147 ([M]$^-$, ^{15}N-MeAsp, 100.00%); the ^{15}N enrichment was 85.71%; the mole peak of the ^{14}N 2-MeAsp was checked by independent FAB$^-$.

NMR Measurements. The liquid-state ^1H and ^{15}N NMR spectra were measured using a Bruker AMX 500 spectrometer (500.13 MHz for ^1H, 50.68 MHz for ^{15}N) equipped for low-temperature NMR down to 100 K. The ^1H spectra were referenced to tetramethylsilane (TMS) by using acetonitrile-d_3 (1.94 ppm), dichloromethane-d_2 (5.31 ppm), dimethylsulfoxide-d_6 (2.50 ppm), methanol-d_3/d_4 (3.31 ppm), and tetrahydrofuran (THF)-d_8 (3.58 ppm) signals as internal references. In the case of the freonic mixtures the central component of the $CHClF_2$ triplet was set to 7.18 ppm.[46] The recycle time was 3 s. In methanol-d_3 (CD_3OH) the hydroxyl signal (−OH) was suppressed by using an jump and return method.[54,55] Standard inverse ^1H-decoupled ^{15}N NMR spectra were recorded with a recycle time of 3 s.

In order to reference the ^{15}N chemical shifts we have recorded under the same ^2H field locking conditions ^{15}N spectra of neat nitromethane containing a capillary with the various deuterated solvents. As the preparation of a capillary using freonic mixtures was difficult, the ^{15}N referencing of the freonic samples was done without ^2H field locking. In the case of acetonitrile the ^{15}N signal was used as internal reference, which resonates at 204.07 ppm[56] with respect to external solid $^{15}NH_4Cl$ scale. To convert the ^{15}N chemical shifts from the nitromethane scale into the external solid $^{15}NH_4Cl$ scale the relation $\delta(CH_3{}^{15}NO_2, \text{liquid}) = \delta(^{15}NH_4Cl, \text{solid}) - 341.168$ ppm was used.[57]

NMR Samples. 1. Solution of the 1−Acid Complexes in Liquefied Freonic Mixture. The pyridine ^{15}N-labeled 5′-triisopropyl-silyl ether of *N*-(pyridoxylidene)-tolylamine (**1a**) and its 1:1 acid−base complexes **1a**−^{15}N-triphenylmethanole (**1b**), **1a**−^{15}N-phenol (**1c**), **1a**−^{15}N-acetic acid (**1d**), **1a**−^{15}N-formic acid (**1e**), **1a**−^{15}N-chloroacetic acid (**1f**), **1a**−^{15}N-dichloroacetic acid (**1g**), **1a**−^{15}N-trifluoroacetic acid (**1h**), **1a**−^{15}N-perfluorobutyric acid (**1i**), and the 1:2 **1a**−^{15}N-dichloroacetic acid (**1j**)

(49) Juaristi, E.; Lopez-Ruiz, H.; Madrigal, D.; Ramirez-Quiros, Y.; Escalante, J. *J. Org. Chem.* **1998**, *63*, 4706−4710.
(50) Aebi, J. D.; Seebach, D. *Helv. Chim. Acta* **1985**, *68*, 1507−1518.
(51) Fadel, A.; Salaun, J. *Tetrahedron Lett.* **1987**, *28*, 2243−2246.
(52) Cativiela, C.; Diaz-de-Villegas, M. D.; Galvez, J. A.; Lapena, Y. *Tetrahedron* **1997**, *53*, 5891−5898.
(53) Sasaki, H.; Carreira, E. M. *Synthesis* **2000**, 135−138.
(54) Gueron, M.; Plateau, P.; Decorps, M. *Prog. Nucl. Magn. Reson. Spectrosc.* **1991**, *23*, 135−209.
(55) Plateau, P.; Gueron, M. *J. Am. Chem. Soc.* **1982**, *104*, 7310−7311.
(56) Briggs, J. M.; Farnell, L. F.; Randall, E. W. *J. Chem. Soc., Chem. Commun.* **1971**, 680−681.
(57) Hayashi, S.; Hayamizu, K. *Bull. Chem. Soc. Jpn.* **1991**, *64*, 688−690.

are prepared as follows. The acids, diluted in dichloromethane-d_2, are added to 1.7 mg (4 μmol) of **1a**−^{15}N, which was in excess; only in the case of **1j** more acid than base was added. Afterward the deuterated liquefied freonic mixture is condensed into the sample tube at 77 K. The solution volume required for these tubes was ∼0.4 mL, it corresponds to ∼10 mM of **1a**.

2. Solution of the 2−Acid Complexes in Organic Solvents. ^{1}H and ^{15}N NMR spectra of doubly ^{15}N-labeled *N*-(pyridoxylidene)-methylamine (**2a**) and its **2a**−^{15}*N*-perfluorobutyric acid adduct (**2b**) were recorded in dichloromethane-d_2 (^{1}H, 4 mM; ^{15}N, 10 mM; 240−190 K), in tetrahydrofuran-d_8 (^{1}H, 2 mM; ^{15}N, 12 mM; 240−170 K), acetonitrile-d_3 (^{1}H, 26 mM; ^{15}N, 26 mM; 235 K) and methanol-d_3 (^{1}H, 7 mM; ^{15}N, 7 mM; 190 K, slow exchange regime is reached with the protic solvent). In addition, **2a** was measured in methanol-d_4 with a deuteration fraction of $\chi_D = 0.99$. The deuteration was done by dissolving **2a** several times in methanol-d_1 and drying it at room temperature in high vacuum overnight. The deuteration fraction in dichloromethane-d_2 achieved was $\chi_D = 0.65$ as estimated by ^{1}H NMR. The deuterated **2a**-trifluoroacetic acid-d_1 (**2c**) was prepared by adding an equimolar ratio of acid to deuterated **2a**, which increased the deuteration fraction to $\chi_D = 0.80$. Comparison with the undeuterated **2a** identifies the δ(OD$\underline{\text{N}}$) chemical shift. Generally the nitrogen signals are identified by recording in addition the non-^{1}H-decoupled ^{15}N NMR spectra and/or by repeating the experiments under the same conditions with samples ^{15}N-labeled only in the imino position.

^{1}H NMR spectra of doubly ^{15}N-labeled **2a** in the liquefied freonic mixtures were recorded at 210−110 K. In the freon mixture at lower temperature **2a** was less soluble, which made all attempts to detect ^{15}N unsuccessful.

3. Solution of the Amino Acid−Substrate in Methanol. ^{1}H and ^{15}N NMR spectra of the Schiff base containing the ^{15}N-labeled 2-MeAsp (**3a**) and its **3a**−perfluorobutyric acid adduct (**3b**) in methanol-d_3 were recorded at 190 K, where on the NMR time scale the slow exchange regime with the protic solvent is reached. **3a** was formed *in vitro* in methanol-d_3 by reacting for 2 h an excess of neutralized pyridoxal with ^{15}N-labeled 2-MeAsp. The formation of **3b** was done by adding the acid diluted in methanol-d_3 to **3a**.

Ab Initio Calculations. Theoretical calculations were performed at the HF level of theory, combined with the standard basis set 6-311+G-(d,p),[58] using the Gaussian 98 program[59] on an Origin 3400 (SGI) computer with 36 MIPS R14000 processors and 20 GB of memory. No symmetry conditions were presumed when starting the optimization of geometry. All minimum-energy structures were checked by vibrational analysis to ensure that the geometry represents a local energy minimum. Zero-point vibrational energy (ZPVE) corrections were included using harmonic frequencies evaluated at the HF/6-311+G-(d,p) level of theory. The geometry optimizations were followed by a single-point energy calculation using a more flexible basis set, namely, 6-311++G(3df,2p);[60] this leads to the protocol of HF/6-311++G(3df,-2p)//HF/6-311+G(d,p), which is proven to achieve reliable accuracy in the calculation of the interaction energies of hydrogen-bonded clusters.[61,62] The interaction energy ΔE_e without ZPVE was calculated from the following relation,

$$\Delta E_e = E(\text{cluster}) - E(\text{SB}) - E(\text{A}) \quad (1)$$

where the total energies are defined as follows: E(cluster) is the energy of the complete hydrogen-bonded cluster, E(SB) is the energy of the corresponding free Schiff base, and E(A) is the energy of the free acid or the acid−imidazole moieties optimized independently at the same level of theory. The basis set superposition error (BSSE) to the interaction energies was estimated using the counterpoise method of Boys and Bernardi.[63−65]

Theoretical Section

Geometric and NMR Hydrogen Bond Correlations. In previous work, it has been shown that the valence bond orders p_i defined by Pauling[66] are useful for describing geometric correlations of hydrogen bonds of the general type A−H···B.[67,68]

$$p_1 = \exp\{-(r_1 - r_1^{\circ})/b_1\} \quad \text{and} \quad p_2 = \exp\{-(r_2 - r_2^{\circ})/b_2\} \quad (2)$$

Here, $r_1 = r_{AH}$ represents the A···H distance, $r_2 = r_{HB}$ represents the H···B distance, p_1 and p_2 represent the corresponding valence bond orders of the diatomic units. Whereas r_1° and r_2° represent the equilibrium distances in the fictive free diatomic units AH and HB, b_1 and b_2 are the parameters describing the decays of the bond order when the bond is stretched. Usually,[66,69] it is assumed that the total bond order to hydrogen is unity

$$p_1 + p_2 = 1 \quad (3)$$

from which it follows that r_1 and r_2 are correlated.

Recently, it was assumed that these equations are only valid for equilibrium geometries where anharmonic zero-point vibrations are neglected.[24,25] In order to take the latter ones into account, the following empirical bond order equations for the equilibrium bond orders were proposed.[24,25]

$$p_1^{H} = p_1 - c^{H}(p_1p_2)^f(p_1 - p_2) - d^{H}(p_1p_2)^g = \exp\{-(r_1^{H} - r_1^{\circ})/b_1\}$$

$$p_2^{H} = p_2 + c^{H}(p_1p_2)^f(p_1 - p_2) - d^{H}(p_1p_2)^g = \exp\{-(r_2^{H} - r_2^{\circ})/b_2\} \quad (4)$$

Expressing the correlation in terms of the normal coordinates, defined as $q_1 = {}^1/_2(r_1 - r_2)$ and $q_2 = r_1 + r_2$, is useful. For a linear hydrogen bond, q_1 represents the distance of the proton from the hydrogen bond center, and q_2 represents the distance between the heavy atoms A and B. Note that the correlation is independent from the hydrogen bond angle. Typical correlation curves[24] of q_2 versus q_1 without and with quantum correction will be presented later in Figure 4. Throughout this work, A−H···B corresponds to the inter- and intramolecular OHN hydrogen bonds in the Schiff base model complexes (Scheme 4); A is the oxygen of the carboxylic acid or the phenolic group, and B is the ring or imino nitrogen of the Schiff bases. We use throughout this paper the corrected bond valences in order to describe experimental data, because the equilibrium bond valences can be used only as an approximation.

(58) Hehre, W. J.; Ditchfield, R.; Pople, J. A. *J. Chem. Phys.* **1972**, *56*, 2257−2261.
(59) Frisch, M. J.; Pople, J. A. *Gaussian98*, 98 ed.; Gaussian, Inc.: Pittsburgh, PA, 1998.
(60) Krishnan, R.; Binkley, J. S.; Seeger, R.; Pople, J. A. *J. Chem. Phys.* **1980**, *72*, 650−654.
(61) González, L.; Mó, O.; Yáñez, M. *J. Chem. Phys.* **1998**, *109*, 139−150.
(62) González, L.; Mó, O.; Yáòez, M.; Elguero, J. *J. Mol. Struct. THEOCHEM* **1996**, *371*, 1−10.
(63) Boys, S. F.; Bernardi, F. *Mol. Phys.* **1970**, *19*, 553−566.
(64) Kim, K. S.; Tarakeshwar, P.; Lee, J. Y. *Chem. Rev.* **2000**, *100*, 4145−4185.
(65) van Duijneveldt, F. B.; van Duijneveldt-van de Rijdt, J. G. C. M.; van Lenthe, J. H. *Chem. Rev.* **1994**, *94*, 1873−1885.
(66) Pauling, L. *J. Am. Chem. Soc.* **1947**, *69*, 542−553.
(67) Steiner, T. *Angew. Chem., Int. Ed.* **2002**, *41*, 48−76.
(68) Steiner, Th. *J. Phys. Chem. A* **1998**, *102*, 7041−7052.
(69) Brown, I. D. *Acta Crystallogr., Sect. B* **1992**, *B48*, 553−572.

In addition, the bond orders are useful in order to derive correlations of NMR parameters with hydrogen bond geometries.[24−29] The following relations were proposed for the chemical shifts of OHN hydrogen bonds

$$\delta(\mathrm{OH\underline{N}}) = \delta(\mathrm{N})^{\circ} p_{\mathrm{OH}}{}^{\mathrm{H}} + \delta(\mathrm{HN})^{\circ} p_{\mathrm{HN}}{}^{\mathrm{H}} + 4\,\delta(\mathrm{OHN})^{*} p_{\mathrm{OH}}{}^{\mathrm{H}} p_{\mathrm{HN}}{}^{\mathrm{H}} \quad (5)$$

$$\delta(\mathrm{O\underline{H}N}) = \delta(\mathrm{OH})^{\circ} p_{\mathrm{OH}}{}^{\mathrm{H}} + \delta(\mathrm{HN})^{\circ} p_{\mathrm{HN}}{}^{\mathrm{H}} + 4\,\delta(\mathrm{OHN})^{*} p_{\mathrm{OH}}{}^{\mathrm{H}} p_{\mathrm{HN}}{}^{\mathrm{H}} \quad (6)$$

$$^{1}J(\mathrm{O\underline{HN}}) = {}^{1}J(\underline{\mathrm{HN}})^{\circ} p_{\mathrm{HN}}{}^{\mathrm{H}} - 8\,{}^{1}J(\mathrm{O\underline{HN}})^{*} (p_{\mathrm{OH}}{}^{\mathrm{H}})^{2} p_{\mathrm{HN}}{}^{\mathrm{H}} \quad (7)$$

The pK_a values associated with the acidic protons in the acid−base complexes can be related to $q_1{}^{\mathrm{H}}$.[24,28,42]

$$\mathrm{p}K_{\mathrm{a}} = A - B q_1{}^{\mathrm{H}} \quad (8)$$

Here, $\delta(\underline{\mathrm{N}})^{\circ}$, $\delta(\underline{\mathrm{HN}})^{\circ}$, $\delta(\underline{\mathrm{OH}})^{\circ}$, $\delta(\underline{\mathrm{H}}\mathrm{N})^{\circ}$, and $^{1}J(\underline{\mathrm{HN}})^{\circ}$ represent the parameters of the fictive free molecular units into which the OHN hydrogen bond can formally dissociate. $\delta(\mathrm{OH\underline{N}})^{*}$, $\delta(\mathrm{O\underline{H}N})^{*}$, and $^{1}J(\mathrm{O\underline{HN}})^{*}$ are the "excess" terms which describe the deviation of the quasi-symmetric hydrogen bond from the average of the fictive limiting molecular units. The parameters used in this work were obtained from previous studies[24,28,40,42] on selected model systems and are discussed below.

In the case of a fast equilibrium between two tautomeric forms α and β (Scheme 2) any observed NMR chemical shift or coupling constant represents a weighed average over both forms characterized by the mole fractions $x(\alpha)$ and $x(\beta)$, e.g.,

$$\delta_{\mathrm{obs}} = x_{\alpha}\delta_{\alpha} + x_{\beta}\delta_{\beta} = \frac{\delta_{\alpha} + K\delta_{\beta}}{1 + K} \quad (9)$$

However, if an equilibrium situation has been proven, then the chemical shifts and the coupling constants provide information about the equilibrium constant K. For this purpose, we rewrite eq 9, which leads to expressions such as

$$K = \frac{x_{\beta}}{x_{\alpha}} = \frac{\delta(\mathrm{OHN})_{\mathrm{obs}} - \delta(\mathrm{OHN})_{\alpha}}{\delta(\mathrm{OHN})_{\beta} - \delta(\mathrm{OHN})_{\mathrm{obs}}} = \frac{{}^{1}J(\mathrm{O\underline{HN}})_{\mathrm{obs}} - {}^{1}J(\mathrm{O\underline{HN}})_{\alpha}}{{}^{1}J(\mathrm{O\underline{HN}})_{\beta} - {}^{1}J(\mathrm{O\underline{HN}})_{\mathrm{obs}}} \quad (10)$$

Here, we identify form α with the enolimine and form β with the iminiophenoxide tautomers. A similar equation can be written for the vicinal three-bond coupling constant. It is then easy to show that both couplings depend linearly of each other

$$^{1}J_{\mathrm{obs}} = {}^{3}J_{\mathrm{obs}}\frac{({}^{1}J_{\beta} - {}^{1}J_{\alpha})}{({}^{3}J_{\beta} - {}^{3}J_{\alpha})} - \frac{{}^{1}J_{\beta}{}^{3}J_{\alpha} + {}^{1}J_{\alpha}{}^{3}J_{\beta}}{({}^{3}J_{\beta} - {}^{3}J_{\alpha})}, \quad \text{with}$$
$$^{1}J \equiv {}^{1}J(\mathrm{OHN}) \quad \text{and} \quad {}^{3}J \equiv {}^{3}J(\mathrm{H_{\alpha}CNH}) \quad (11)$$

A problem for the calculation of K from observed NMR parameters is that the intrinsic coupling constants in these equations depend on the solvent, static dielectric constant,[70−74] and temperature.[40]

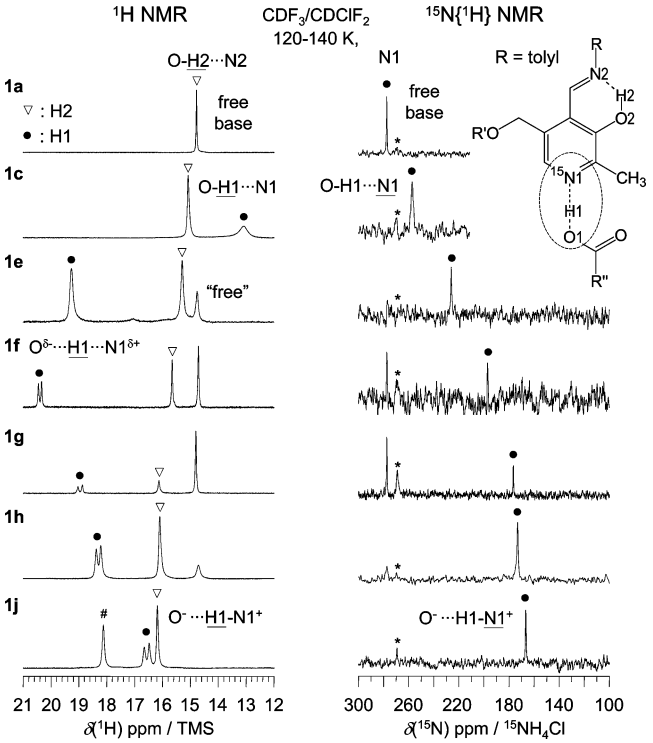

Figure 1. ^{1}H and ^{15}N {^{1}H} NMR of the selectively ^{15}N-labeled in ring position **1a**−acid adducts (R = tolyl, R′ = Si(CH(CH$_3$)$_2$)$_3$) with a variety of halogenated acetic acid derivatives and alcohols **1a**−**1j** in liquefied freonic mixtures of $CDF_3/CDClF_2$ at 140−120 K. Values are listed in Table 1. Symbols: ● corresponds to the intermolecular O1H1N1 hydrogen bond; ▽ corresponds to the intramolecular O2H2N2 hydrogen bond of **1** involved in the complex; nonmarked signals belong to the free base; #, signal at 18.12 ppm of $[(CHCl_2CO_2)_2H]^-$ from the 2:1 acid−base complex with dichloroacetic acid (**1j**); ∗, impurity.

Results

NMR Spectroscopy. The results of the NMR experiments are depicted in Figures 1 and 2. All parameters obtained are collected in Tables 1−3.

Acid−Base Complexes of 1 in $CDF_3/CDClF_2$. Figure 1 depicts the low-temperature ^{1}H and ^{15}N {^{1}H} NMR spectra of the aldenamine Schiff base **1a** and its 1:1 complexes with various proton donors dissolved in $CDF_3/CDClF_2$. **1a** was selectively ^{15}N-labeled in the pyridine ring. Under these experimental conditions, the regime of slow hydrogen bond exchange is realized, i.e., the signals observed are the intrinsic signals of the intermolecular 1:1 acid−base complexes.

When the acidity of the carboxylic acid[75−77] is increased, the ^{1}H signal of the intermolecular O1H1N1 hydrogen bond is shifted from almost 13.1 ppm to a maximum of 20.4 ppm and then back to 16.6 ppm where a doublet splitting arises from

(70) Morgan, S. O.; Lowry, H. H. *J. Phys. Chem.* **1930**, *34*, 2385−2432.
(71) Isnardi, H. *Z. Phys.* **1922**, *9*, 153−179.
(72) Le Fevre, R. J. W. *Trans. Faraday Soc.* **1938**, *34*, 1127−1132.
(73) Carvajal, C.; Tolle, K. J.; Smid, J.; Szwarc, M. *J. Am. Chem. Soc.* **1965**, *87*, 5548−5553.
(74) Cappelli, C.; Mennucci, B.; Cammi, R.; Rizzo, A. *J. Phys. Chem. B* **2005**, *109*, 18706−18714.
(75) Polansk, J.; Bak, A. *J. Chem. Inf. Comput. Sci.* **2003**, *43*, 2081−2092.
(76) Kortüm, G.; Vogel, N.; Andrussow, K. *Dissociation Constants of Organic Acids in Aqueous Solutions*; London, 1961.
(77) Vcelakova, K.; Zuskova, I.; Kenndler, E.; Gas, B. *Electrophoresis* **2004**, *25*, 309−317.

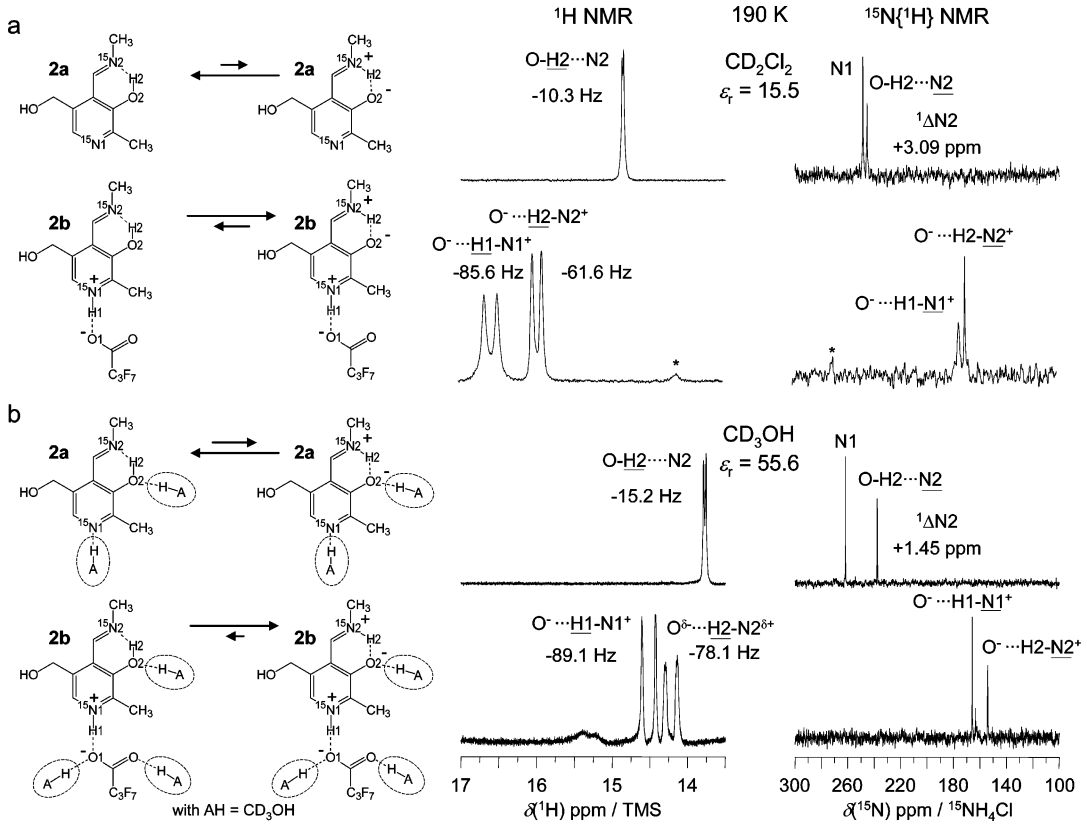

Figure 2. ^{15}N {^{1}H} and ^{1}H NMR of the doubly ^{15}N-labeled aldimine Schiff base **2a** and its 1:1 **2a**−perfluorobutyric acid complex (**2b**) at 190 K: (a) in dichloromethane-d_2; (b) in methanol-d_3. ∗: signal of free **2a**. Values are listed in Table 2.

Table 1. NMR Parameters of the Intermolecular O1H1N1 Hydrogen Bond of **1**[a−e]

complex		pK_a -O1H1[a]	solvent	T /K	δ(O1H1N1) /ppm	^1J(O1H1N1) /Hz	δ(O1H1N1) /ppm
1a[d]	**1a**[e]		freon	140			277.44(−5.06)[b]
1a + triphenylmethanol	**1b**	12.73	freon	120	9.04		264.95(−17.55)[b]
1a + phenol	**1c**	9.89	freon	120	13.10		257.31(−25.19)[b]
1a + acetic acid	**1d**	4.75	freon	120	16.58		248.35(−34.15)[b]
1a + formic acid	**1e**	3.75	freon	130	19.52		226.15(−56.35)[b]
1a + chloroacetic acid	**1f**	2.85	freon	140	20.40	−57.56	197.41(−85.08)[b]
1a + dichloroacetic acid	**1g**	1.48	freon	120	18.96	−79.75	176.50(−106.00)[b]
1a + trifluoroacetic acid	**1h**	0.52	freon	140	18.29	−83.33	173.26(−109.24)[b]
1a + perfluorobutyric acid	**1i**	0.17	freon	125	18.00	−83.60	171.77(−110.72)[b]
1a + dichloroacetic acid[c]	**1j**		freon	130	16.57	−88.24	166.69(−115.81)[b]

[a] pK_a values in aqueous solution of the acid proton H1 are obtained from refs 75−77. [b] Values in brackets with respect to **1a** in the organic solid state, resonating at 282.5 ppm with respect to external solid $^{15}NH_4Cl$ (ref 42). [c] 2:1 dichloroacetic acid−**1a** complex, with a proton signal at 18.12 ppm of $[(CHCl_2CO_2)_2H]^-$. [d] The H2 signal of the intramolecular hydrogen bond appears at 14.8−16.2 ppm. [e] With δ(O2H2N2) = 260.01(−19.49) ppm and δ(O2H2N2) = 14.78 ppm, for further information see the Supporting Information. ^{1}H and ^{15}N chemical shifts are with respect to internal TMS and external solid $^{15}NH_4Cl$, respectively.

coupling with the pyridine ^{15}N. At the same time, the corresponding ^{15}N signal is shifted monotonically from 277.4 to 166.7 ppm. These findings indicate a continuous shift of the proton position from oxygen to nitrogen, as in the case of pyridine−acid complexes.[32,33] For the zwitterionic states of **1f**−**1i** values of ^1J(O1H1N1) between −57 to −83 Hz are typical.

Simultaneously, the signal of the proton in the intramolecular O2H2N2 hydrogen bond is only slightly shifted from 14.8 to 16.2 ppm. Additional experiments of ^{15}N-imino labeled **1a** (Figure S1 in the Supporting Information) indicate that this shift is not associated with the appearance of a splitting with the ^{15}N imino nitrogen. Thus, this effect arises only from an elongation of the phenolic OH bond, not from a shift of the keto−enol tautomerism.

When dichloroacetic acid is added in excess, the 2:1 acid−base complex **1j** is formed as depicted in the bottom spectra of Figure 1. It is characterized by a doublet for the O1H1N1 hydrogen bond, a singlet for the O2H2N2 hydrogen bond, and a signal at 18.12 ppm for the OHO hydrogen bond between the two carboxylic acid moieties. The observed coupling constant of −88.24 Hz of **1j** is larger than in the corresponding 1:1 complex of **1g**, indicating that the proton-donating power of the linear acid dimer is larger than that of the monomer. We note that similar effects have been observed previously for pyridine.[33] The interested reader can find the complete set of ^{15}N spectra for all compounds in the Supporting Information, depicted in Figure S2.

1:1 Acid−Base Complexes of 2. Whereas protonation of the pyridine ring had little effect on the intramolecular O2H2N2 hydrogen bond of **1**, different behavior was observed for **2**, which has a more basic imino nitrogen than **1**.

Table 2. $^{1}H/^{15}N$ Chemical Shifts, One-Bond ^{1}J(OHN) and Three-Bond (Vicinal) $^{3}J(H_{\alpha}CNH2)$ Coupling Constants and One-Bond Secondary Isotope Effects $^{1}\Delta N(D) = \delta(ODN) - \delta(OHN)$ of the Schiff Base **2a** without and with Perfluorobutyric Acid (**2b**), Trifluoroacetic Acid-d_1 (**2c**), and the Amino Acid−Substrate (**3a**) and Its Complex with Perfluorobutyric Acid (**3b**) in a Variety of Solvents[a−m]

	solvent	T /K	ϵ_r[m]	K	$\delta(^{1}H)$ O2H2N2 /ppm	^{1}J(H,N) O2H2N2 /Hz	^{3}J(H,H) $H_{\alpha}CNH2$ /Hz	$\delta(^{15}N)$ O2H2N2 /ppm[c]	$^{1}\Delta N2(D$ /ppm	$\delta(^{1}H)$ O1H1N1 /ppm	^{1}J(H,N) O1H1N1 /Hz	$\delta(^{15}N)$ O1H1N1 /ppm[d]
2a[h]	freon	210	∼13	4.76[i]	14.97	−8.90						
	freon	200	∼15	5.00[i]	15.03	−10.18						
	freon	190	∼16	5.26[i]	15.10	−11.52						
	freon	180	∼18	5.56[i]	15.17	−12.99						
	freon	170	∼20	5.88[i]	15.23	−14.68						
	freon	160	∼22	6.25[i]	15.30	−16.66						
	freon	150	∼24	6.67[i]	15.47	−19.81						
	freon	120	∼34	8.33[i]	15.82	−29.62						
	freon	110	∼39	9.09[i]	15.87	−37.27						
2a[g]	CD_2Cl_2	240	11.8		14.54			253.56(−25.94)	3.20			275.58(−6.91)
	CD_2Cl_2	230	12.4	0.08[i]	14.61	−5.61		252.28(−27.22)	3.19			273.53(−8.97)
	CD_2Cl_2	220	13.1	0.09[i]	14.67	−6.67		250.68(−28.82)	3.24			271.37(−11.13)
	CD_2Cl_2	210	13.8	0.11[i]	14.73	−7.84		248.90(−30.59)	3.17			269.37(−13.12)
	CD_2Cl_2	200	14.6	0.13[i]	14.79	−9.03		246.82(−32.67)	3.13			267.57(−14.93)
	CD_2Cl_2	190	15.5	0.15[i]	14.85	−10.30		244.85(−34.65)	3.09			266.52(−15.98)
2b	CD_2Cl_2	240	11.8	0.47[j]	15.82	−34.83						
	CD_2Cl_2	230	12.4	0.57[j]	15.84	−38.26						
	CD_2Cl_2	220	13.1	0.69[j]	15.86	−42.12	6.27					
	CD_2Cl_2	210	13.8	0.85[j]	15.87	−46.15	7.01					
	CD_2Cl_2	200	14.6	1.04[j]	15.87	−50.34	7.64					
	CD_2Cl_2	190	15.5	1.85[j]	15.96	−61.62	8.28	174.12(−105.3 8)		16.57	−85.55	169.48(−113.01)
2c[b]	CD_2Cl_2	190	15.5		15.96	−62.84		171.85(−107.6 5)[e]	−3.54[e]	16.78	−84.20	164.92(−117.58)[e,f]
2a	THF-d_8	240	9.6		14.03			257.56(−21.94)				286.56
	THF-d_8	230	10.1		14.07			257.62(−21.88)				286.46
	THF-d_8	220	10.6		14.11			257.59(−21.91)				286.32
	THF-d_8	210	11.2		14.14			257.63(−21.87)				286.17
	THF-d_8	200	11.8		14.18			257.64(−21.86)				286.00
	THF-d_8	190	12.5		14.22			257.67(−21.83)				285.85
	THF-d_8	180	13.3		14.25			257.68(−21.81)				285.66
	THF-d_8	170	14.1		14.29			257.69(−21.81)				285.42
2b	THF-d_8	240	9.6	0.29[j]	15.44	−27.07						
	THF-d_8	230	10.1	0.43[j]	15.57	−33.20						
	THF-d_8	220	10.6	0.56[j]	15.65	−38.12	5.84					
	THF-d_8	210	11.2	0.76[j]	15.69	−44.00	6.70			19.19		
	THF-d_8	200	11.8	1.03[j]	15.67	−50.06	7.53	186.00(−93.50)[k]		19.11		182.50(−100.00)[l]
	THF-d_8	190	12.5	1.34[j]	15.63	−55.33	8.47	180.91(−98.59)[k]		19.01		180.63(−101.87)[l]
	THF-d_8	180	13.3	1.76[j]	15.55	−60.68	9.42	175.85(−103.6 5)[k]		18.93	−77.73	178.91(−103.59)[l]
	THF-d_8	170	14.1	2.43[j]	15.45	−66.41	10.53	162.43(−117.0 8)		18.83	−78.66	176.52(−105.98)
2a	CD_3CN	235	∼36.6		14.49			254.58(−24.92)				283.43
2b	CD_3CN	235	∼36.6		15.52	−68.92		167.00(−112.5 0)		15.00	−82.58	163.58(−118.92)
2a	CD_3OH	190	55.6		13.77	−15.25		237.64(−41.86)	1.45[g]			261.74(−20.76)
2b	CD_3OH	190	55.6		14.22	−78.12	11.84	154.24(−125.3 0)		14.51	−89.12	165.96(−116.53)
3a	CD_3OH	190	55.6		13.88	−18.48		231.75(−47.75)				
3b	CD_3OH	190	55.6		15.22	−54.49		184.07(−95.43)		14.94		

[a,b] ^{1}H and ^{15}N chemical shifts are with respect to internal TMS and external solid $^{15}NH_4Cl$, respectively. The comparison with the undeuterated **2a** identifies δ(ODN). The deuteration fractions χ_D were estimated by integration of the ^{1}H signals 0.65 (*a*) and 0.80 (*b*). [c] Values in brackets with respect to the neat methoxy-protected Schiff base, namely, *N*-(2-methoxybenzylidene)-methylamine, resonating at 279.5 ppm with respect to external solid $^{15}NH_4Cl$ (ref 40). [d] Values in brackets with respect to **1a** in the organic solid state, resonating at 282.5 ppm with respect to external solid $^{15}NH_4Cl$ (ref 42). [e] Obtained from simulated ^{15}N spectra by using the ^{1}J(OHN) from the corresponding ^{1}H spectra; for further details, see the Supporting Information. [f] With $^{1}\Delta N1(D)$ of −0.82 ppm. [g] Obtained from **2a** in CD_3OD at 190 K. [h] Couplings not observable at 140−130 K. *K* is calculated by using eq 10; the limiting values were obtained similar as described in ref 40. [i] $^{1}J(O2H2N2)_{\alpha} = 0$ Hz (−24 ppm) and $^{1}J(O2H2N2)_{\beta} = -77$ Hz (−121 ppm). [j] $^{1}J(O2H2N2)_{\alpha} = -9$ Hz (−44 ppm) and $^{1}J(O2H2N2)_{\beta} = -90$ Hz (−138 ppm). [k] Values predicted from ^{1}J(O1H1N1) by using eq 7. [l] Values predicted from δ(O1H1N1) by using eq 5. [m] Temperature dependence on the static dielectric constant ϵ_r of CH_2Cl_2 (ref 70), CH_3OH (refs 71 and 72), THF (ref 73), and CH_3CN(RT) (ref 74) by fitting the experimental values with relations described in ref 40; the values of the freon mixture are approximately mentioned by using the empirical relation from ref 46.

The ^{1}H and ^{15}N spectra of the doubly ^{15}N-labeled aldimine Schiff base **2a** and of its 1:1 complex **2b** with perfluorobutyric acid are depicted in Figure 2, parts a and b. The experimental temperature was 190 K.

In the case of CD_2Cl_2 as solvent (Figure 2a) the O2H2N2 signal of the aldimine Schiff base **2a** at 14.8 ppm is split into a doublet by scalar coupling with the imino ^{15}N; the coupling constant is −10.3 Hz. The formation of the complex with perfluorobutyric acid **2b** leads to a low-field shift to 15.9 ppm and an increase of the coupling constant to −61.6 Hz. Simultaneously, the O1H1N1 signal appears at 16.6 ppm, exhibiting a coupling constant of −85.5 Hz with the pyridine ^{15}N. Whereas in **2a** both the pyridine and imino nitrogen signals appear at low field, they are shifted in the adduct **2b** to substantially higher field, indicating protonation of both nitrogen atoms.

Deuteration of the mobile proton sites leads to a low-field shift δ(O2D2N2) − δ(O2H2N2) of +3.09 ppm for **2a**, and a

Table 3. Interaction Energies, Selected Structural H-Bonds, and Predicted NMR Parameters of the Model Schiff Base Adducts at the HF Level of Theory[a−c]

	2c(OH,OH)	**2c**(OH,NH)	**2d**(OH,NH)	**2c**(NH,OH)	**2c**(NH,NH)	**2d**(NH,NH)
ΔE_e^N/kJ mol^{-1}	−40.71	−52.68	−53.18	−13.02	−19.19	−40.12
ΔE_e^B/kJ mol^{-1}	−36.76	−51.14	−52.91	−10.79	−17.07	−39.21
ΔE_0/kJ mol^{-1}	−35.91	−47.73	−48.03	−11.88	−17.14	−32.91
$\Delta\epsilon$(BSSE)/kJ mol^{-1}	3.95	1.54	0.27	2.23	2.12	0.91
r(N1···H1)/Å	1.813	1.807	1.766	1.085	1.084	1.047
r(O1···H1)/Å	0.974	0.975	0.982	1.460	1.465	1.615
δ(O1H1N1)/ppm[b]	−16.6	−16.9	−18.5	−112.2	−112.4	−121.7
δ(O1H1N1)/ppm[c]	6.5	6.6	7.6	16.5	16.4	13.9
r(N2···H2)/Å	1.849	1.003	1.003	1.842	1.004	1.004
r(O2···H2)/Å	1.003	1.897	1.896	0.956	1.890	1.889
δ(O2H2N2)/ppm[b]	−17.1	−154.7	−153.5	−17.2	−152.9	−152.7
δ(O2H2N2)/ppm[c]	11.8	7.6	8.0	11.9	8.3	8.4

[a] Calculated after the protocol HF/6-311++G(3df,2p)//HF/6-311+G(d,p). ΔE_e^N and ΔE_e^B represent the interaction energy without and with the basis set superposition error correction $\Delta\epsilon$(BSSE), respectively. ΔE_0 is the ZPVE-corrected ΔE_e. The frequencies for ZPVE correction were evaluated at the HF/6-311+G(d,p) level of theory. The energy difference of the two tautomeric forms **2a**(OH) and **2a**(NH) is $\Delta E_e = 23.32$ kJ mol^{-1} ($\Delta E_0 = 23.80$ kJ mol^{-1}).[b] The ^{15}N chemical shifts are predicted from the optimized r(N1···H1) distances by using eq 5. [c] The ^{1}H chemical shifts are predicted from the optimized r(N2···H2) distances by using eq 6. Further details can be found in the Supporting Information.

high-field shift of −3.54 ppm in the 1:1 complex **2c** with trifluoroacetic acid-d_1, (Table 2), which is in agreement with a proton preferentially on oxygen in **2a** and on nitrogen in **2c**.[40] The interested reader can find the ^{15}N spectra of the deuterated compounds in Figures S3 and S4 in the Supporting Information.

In methanol-d_3 the O2H2N2 and O2H2N2 signals of **2a** appear at 13.8 and 237.6 ppm, with a coupling constant of −15.2 Hz (Figure 2b). This finding is similar to that with CD_2Cl_2 as solvent. However, a substantial difference is observed for **2b**. In comparison to CD_2Cl_2 as solvent, methanol-d_3 produces large ^{1}H and ^{15}N high-field shifts and increases substantially both ^{1}H−^{15}N coupling constants. The coupling constant ^1J(O2H2N2) exhibits the maximum possible value of −90 Hz,[40] but ^1J(O2H2N2) is only −78 Hz. This indicates that the fast keto−enol tautomerism is still operative and not obliterated as it is in water.[12]

Furthermore, similar results are obtained for the Schiff base **2a** and its adduct **2b** (Table 2) in various organic solvents (i.e., acetonitrile-d_3, methanol-d_3, methanol-d_4, tetrahydrofuran-d_8) and in liquefied freon mixtures. The corresponding spectra can be found in Figures S5−S8 in the Supporting Information.

Methanolic Solutions of the 2-MeAsp Schiff Base 3. We recorded the NMR spectra of the AspAT substrate−mimic Schiff base **3a** with ^{15}N-labeled 2-MeAsp and its perfluorobutyric acid adduct **3b** in methanol-d_3 at 190 K, as shown in Figure S9 of the Supporting Information. The NMR parameters are included in Table 2. It was found that **3** behaves similarly to **2**.

Ab Initio Calculations. Ab initio calculations were performed at the HF level of theory for the Schiff base−trifluoroacetic acid complex **2c** and for the ternary complex with imidazole **2d**. The optimized geometries of the local minima and the corresponding energies were obtained. In addition, selected NMR parameters were predicted from the optimized geometries using eqs 5 and 6. Zero-point vibrational energy (ZPVE) corrections in harmonic approximation were small and therefore neglected. We are aware that anharmonic corrections should be applied, which are, however, beyond the scope of this study. In addition, the basis set superposition errors were found to be small and were, therefore, also neglected.

For the O2H2N2 hydrogen bond stationary points, two local minima were found corresponding to the enolimine form and iminiophenoxide form. Furthermore, two local minima were also

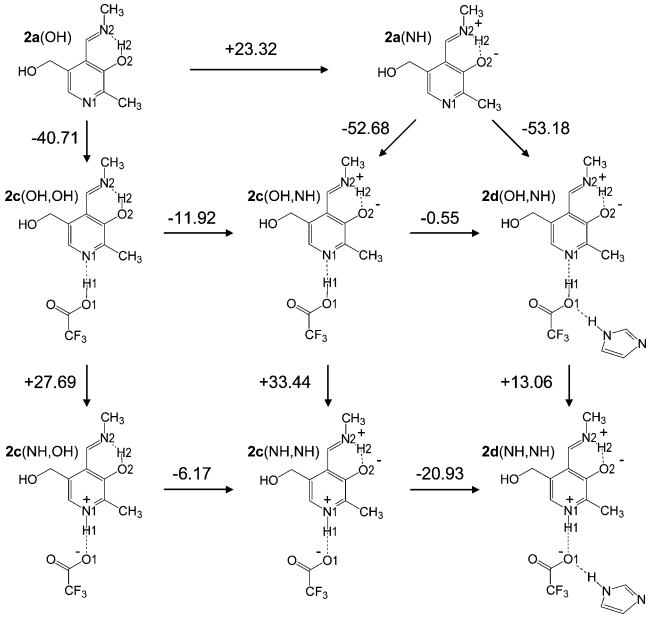

Figure 3. Energy scheme of optimized Schiff base models. Visualized are the at HF/6-311+G(d,p) level of theory optimized Schiff base **2a** in enolimine form **2a**(OH) and ketoimine form **2a**(NH) and its isomeric Schiff base−trifluoroacetic acid adducts **2c**, with the unprotonated pyridine nitrogen **2c**(OH,OH) and **2c**(OH,NH) and protonated pyridine nitrogen **2c**(NH,OH) and **2c**(NH,NH). Also shown are the ternary complexes with imidazole **2d**(OH,NH) and **2d**(NH,NH). The calculated energies ΔE_e^N in kJ mol^{-1} are also shown. All parameters are listed in Table 3.

observed for the O1H1N1 hydrogen bond corresponding to a molecular OH form labeled as **2c**(OH,OH) and **2c**(OH,NH) and a zwitterionic NH form labeled as **2c**(NH,OH) and **2c**(NH,-NH). For the ternary complexes only the optimized structures **2d**(OH,NH) and **2d**(NH,NH) are obtained.

The energies of all structures of the O1H1N1 hydrogen bonds are shown in Figure 3, which illustrated the energy differences between the calculated Schiff base models. All results are collected in Table 3 and in Table S1 of the Supporting Information and will be discussed in the following section.

As expected, shifts of ^{15}N signals to high field result when the N1···H1 distances are shortened. This is observed when the imidazole moiety is added: in structures **2d**(OH,NH) and **2d**(NH,NH), the N1···H1 distance is shortened and the corresponding pyridine ^{15}N signal is shifted to high field (Table 3).

The calculated energy differences between the different structures (Figure 3) indicate that structures **2c**(OH,OH) and **2c**(OH,NH) are both more stable than **2c**(NH,OH) and **2c**(NH,NH). This is a consequence of the low dielectric constant of the gas phase. Additionally, it is interesting to note that the zwitterionic iminiophenoxide forms **2c**(OH,NH) and **2c**(NH,NH) are more stable than the corresponding enolimine forms **2c**(OH,OH) and **2c**(NH,OH), respectively. This effect is a result of the strongly electron-withdrawing nature of the protonated, positively charged imino group. This was also recently recognized experimentally in aldimine model studies in aqueous solution.[12]

Discussion

We have performed low-temperature ^{1}H and ^{15}N liquid-state NMR experiments on Schiff bases of the biologically important cofactor pyridoxal, and their hydrogen-bonded 1:1 complexes with carboxylic acids (Scheme 4). These complexes were designed to model the cofactor PLP in a variety of enzymic environments. In particular, we were interested in the question of whether or not and how in a polar aprotic solution the structures of the functional inter- and intramolecular OHN hydrogen bonds are coupled to each other and how additional hydrogen bonds affect this hydrogen bond coupling. Previously, we had shown that this interaction is present in the organic solid state,[42] but obliterated in aqueous solution,[12] a result that raises the question of which liquid environment mimics best the active site of PLP-dependent enzymes.

In this section, we will first discuss the calculated geometries and ^{1}H/^{15}N chemical shifts of the inter- and intramolecular OHN hydrogen bonds of all model compounds **1**−**3** (Scheme 4) in terms of the hydrogen bond correlation model described in the Theoretical Section. This allows us to verify the coupling of the two OHN hydrogen bonds in terms of average hydrogen bond geometries in polar aprotic solution. Finally, we will discuss potential biological implications arising from these results.

Geometric H-Bond Correlations. The following discussion of the geometries of OHN hydrogen bonds is conveniently based on the proton coordinate $q_1 = {}^1/_2(r_{OH} - r_{HN})$ and the heavy atom coordinate $q_2 = r_{OH} + r_{HN}$ defined in Figure 4. For a linear H-bond, the proton coordinate q_1 corresponds to the deviation of the proton from the hydrogen bond center and the heavy atom coordinate q_2 corresponds to the N···O distance. Previously, based on a collection of neutron structures of various crystals containing OHN hydrogen bonds it was shown that q_2 and q_1 are correlated with each other[24,68] as illustrated in Figure 4. The solid lines correspond to the correlation between the equilibrium hydrogen bond structures according to eq 3, whereas the dotted lines include an empirical quantum-mechanical correction for anharmonic zero-point energy vibrations (eq 4).[24] These curves are general for all OHN hydrogen bonds, i.e., the same in Figure 4, parts a and b, containing the geometric data points for the inter- and the intramolecular OHN hydrogen bonds of **2** calculated in this study using ab initio methods.

Since the data points calculated for both the inter- and the intramolecular OHN bridges were not corrected for anharmonic zero-point vibrations, they are well located on the predicted solid lines, whereas experimental data points are predicted to be located on the dashed lines. Clearly, both the inter- and the intramolecular OHN hydrogen bonds are characterized by two

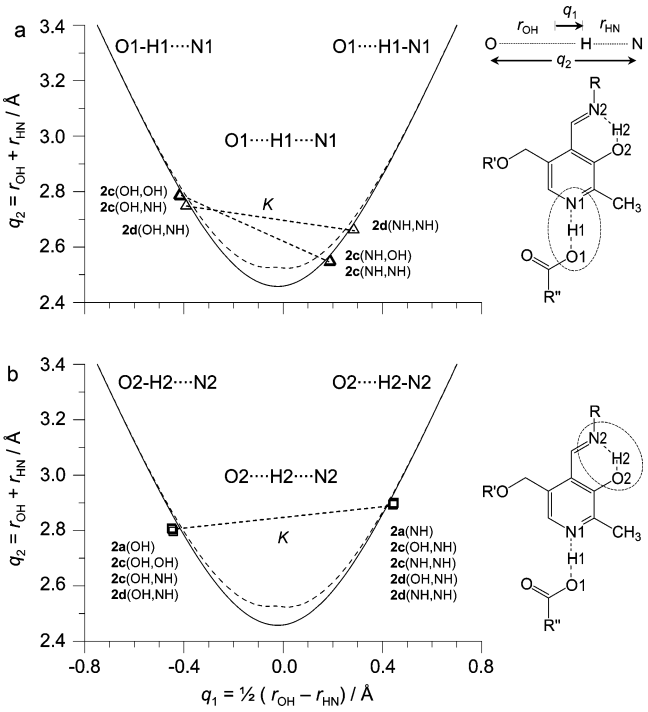

Figure 4. Correlation of the coordinates q_2 vs q_1 of general OHN hydrogen bonds according to ref 24. The solid correlation curve refers to the equilibrium structures, whereas the dashed curve includes an empirical quantum correction for anharmonic ground-state vibrations. The data points refer to the optimized geometries of the model Schiff base adducts indicated at the HF level of theory: (a) data points for the intermolecular O1H1N1 hydrogen bond; (b) data points for the intramolecular O2H2N2 hydrogen bond. For further explanation, see text.

stationary points corresponding to the two tautomeric OH and NH forms linked by dashed straight lines in Figure 4. Formally, these lines correspond to the hydrogen bond coordinates $\bar{q}_1$ and $\bar{q}_2$ averaged over both forms

$$\bar{q}_2 = \frac{q_2^{NH} - q_2^{OH}}{q_1^{NH} - q_1^{OH}}(\bar{q}_1 - q_1^{OH}) + q_2^{OH} \qquad (12)$$

where q_i^{NH} and q_i^{OH}, $i = 1, 2$, correspond to the intrinsic values.

We note that the NH forms of O1H1N1 exhibit smaller values of q_2 and hence smaller absolute values of q_1 as compared to the OH forms, i.e., the NH forms exhibit shorter hydrogen bonds than the OH forms. The opposite result is obtained for the tautomers of O2H2N2. The geometries of both tautomers of O2H2N2 are almost independent of the geometries of the intermolecular O1H1N1 hydrogen bond; a small influence of O2H2N2 on O1H1N1 is observed. However, the different geometries of O1H1N1 affect strongly the equilibrium constants of the tautomerism in O2H2N2 and hence the corresponding reaction enthalpy.

^{1}H−^{15}N Chemical Shift Correlations. The question arises whether the calculated results obtained for the isolated molecules are also valid for condensed phases. In order to answer this question, we have plotted in Figure 5 the experimental and calculated ^{1}H chemical shifts δ(O$\underline{\text{H}}$N) of both OHN hydrogen bonds of all Schiff bases studied as a function of the corresponding ^{15}N chemical shifts δ(OH$\underline{\text{N}}$). Data points on the left sides correspond to molecular complexes where the proton is located close to oxygen, while those on the right side correspond to zwitterionic complexes, and those in the center correspond

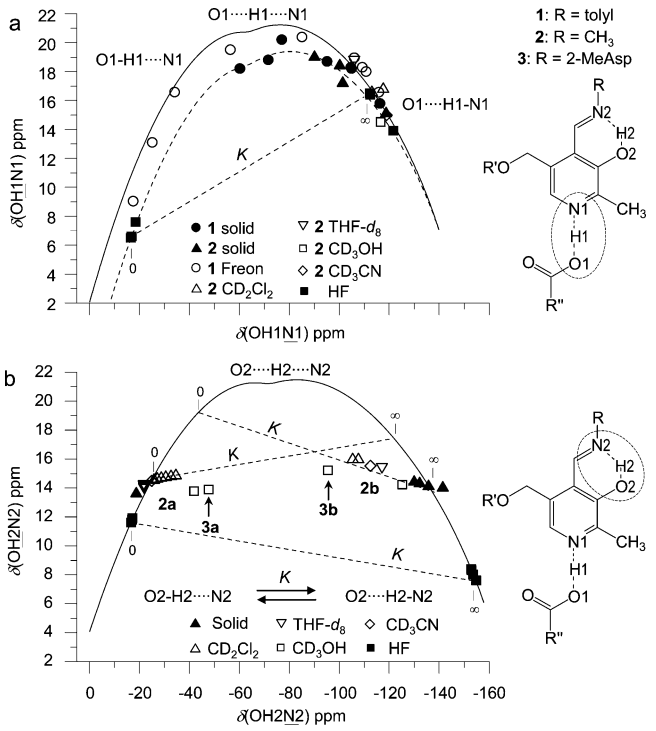

Figure 5. ^{1}H vs ^{15}N chemical shift correlations. Also included are the predicted NMR parameters of the optimized geometries of the model Schiff base adducts at the HF level of theory: (a) shown for the intermolecular O1H1N1 hydrogen bond for **1** and **2**; the values of **1** and **2** in the organic solid state are obtained from ref 42; (b) shown for the intramolecular O2H2N2 hydrogen bond for **2** and **3**. For further explanation, see text.

to strong hydrogen bonds. We have included values obtained recently for the organic solid state.[42]

For a better comparison of different OHN hydrogen-bonded systems, it is convenient to reference the ^{15}N chemical shifts not to a standard such as ammonium chloride but to the value of the nitrogen atom in a non-hydrogen-bonded form. Here, we used the solid compound **1a** (282.5 ppm with respect to external solid $^{15}NH_4Cl$) as a reference for the pyridine-type nitrogen atoms[42] and the methoxy-protected *N*-(2-methoxybenzylidene)-methylamine[40] for the imino nitrogen atoms resonating at 279.5 ppm.

The chemical shift correlations of Figure 5 arise from the fact that $\delta(O\underline{H}N)$ and $\delta(OH\underline{N})$ are measures of the hydrogen bond coordinates q_2 and q_1. When these coordinates increase, the chemical shift changes converge to the limiting values corresponding to the fictive separate diatomic units, which define the position of the two ends of the chemical shift correlation curves. The maxima of the curves are determined by the ^{1}H chemical shift of the strongest quasi-symmetric OHN hydrogen bond.

The correlation lines in Figure 5 were calculated using eqs 5 and 6, including the correction for anharmonic zero-point energy vibrations as described previously[24,42] and in the Theoretical Section, using the parameters assembled in Table 4. The dashed and solid curves in Figure 5a differ in the limiting ^{1}H chemical shifts $\delta(O\underline{H})°$ of the fictive free OH group which was assumed to be -3 ppm for the solid state and $+2$ ppm for the polar solution.[24] This difference leads to a maximum ^{1}H chemical shift of about 21 ppm for freon solution but only of about 19.5 ppm for the solid state. The parameters describing the solid curve in Figure 5b were determined previously for an aromatic Schiff base[42] with slight adjustment to best fit the experimental data points.

The calculated ^{1}H/^{15}N chemical shift correlation curves are valid only in the absence of a proton-transfer equilibrium between two tautomeric forms.[40] Only if the proton always moves in a single well the maximum hydrogen bond compression can be achieved, corresponding to the maximum proton chemical shift in the configuration of the quasi-symmetric H-bond around $q_1 = 0$. In the presence of an equilibrium between OH and NH forms we expect the average chemical shifts

$$\bar{\delta}(O\underline{H}N) = \frac{\delta(O\underline{H}N)^{NH} - \delta(O\underline{H}N)^{OH}}{\delta(OH\underline{N})^{NH} - \delta(OH\underline{N})^{OH}}(\bar{\delta}(OH\underline{N}) - \delta(OHN)^{OH}) + \delta(OHN)^{OH} \quad (13)$$

where the superscripts OH and NH represent the intrinsic chemical shifts of the OH and NH forms given by the chemical shift correlation curves. Equation 13, which is easily derived from eq 9, is represented in Figure 5 by the straight dashed lines labeled with the equilibrium constant K of tautomerism which increases from zero on the left intersection point with the correlation curve to infinity on the right intersection point.

Thus, using eqs 5 and 6 one can transform the observed chemical shifts to the hydrogen bond coordinates q_2 and q_1 of Figure 4. This is of special importance since polar solution NMR parameters are available but no hydrogen bond coordinates.

Next we discuss the results obtained for O1H1N1 depicted in Figure 5a. The solid and dashed correlation curves reproduce well the experimental data measured here for the liquid state and previously[42] for the solid state. No substantial difference from the correlation published previously for pyridine−acid complexes[24] is observed, indicating that the chemical shifts are not influenced strongly by the different chemical structures but mainly by the very similar hydrogen bond acceptor properties of pyridine and of the model Schiff bases studied here.

Figure 5a indicates an important difference between the isolated molecules and those embedded in polar solvent. If there was no difference, the experimental ^{1}H/^{15}N chemical shift data points should be located close to the straight dashed line calculated using eq 13 for the case of tautomerism between molecular OH and a zwitterionic NH forms. The experimental results are, however, not in agreement with this prediction. At an ^{15}N chemical shift of about 80 ppm (i.e., the center of the correlation curve typical for a quasi-symmetric complex), the ^{1}H chemical shifts are larger than predicted by the dashed straight line. This means that instead of an equilibrium between an OH and an NH form where a quasi-symmetric short hydrogen bond corresponds to a saddle point rather than to a minimum, O1H1N1 forms stable strong and short hydrogen bonds. We note that a more detailed study of such a quasi-symmetric short hydrogen bond may reveal a solvent-induced multisite equilibrium between different complexes exhibiting all slightly different low- or no-barrier hydrogen bonds for the proton motion as proposed by Golubev et al.[32] and as demonstrated recently using the isotopic perturbation method by Perrin and co-workers.[78−80]

(78) Perrin, C. L.; Lau, J. S. *J. Am. Chem. Soc.* **2006**, *128*, 11820−11824.
(79) Perrin, C. L.; Lau, J. S.; Ohta, B. K. *Pol. J. Chem.* **2003**, *77*, 1693−1702.
(80) Perrin, C. L; Nielson, J. B. *Annu. Rev. Phys. Chem.* **1997**, *48*, 511−544.

Table 4. Geometrical and NMR Parameters of the OHN Hydrogen Bond Correlations[a,b]

Geometrical Parameters of the OHN Hydrogen Bond								
system	b_{OH} /Å	rOH^o /Å	b_{HN} /Å	rHN^o /Å	f	g	c^H	d^H
OHN[c,d]	0.371	0.942	0.385	0.992	5	2	360	0.7

NMR Parameters of the OHN Hydrogen Bond										
complex	state	OHN	δ(N)^o /ppm	δ(HN)^o /ppm	δ(OHN)* /ppm	δ(OH)^o /ppm	δ(HN)^o /ppm	δ(OHN)* /ppm	^1J(HN)^o /Hz	^1J(OHN* /Hz
Intermolecular O1H1N1 Hydrogen Bond										
1,**2**-HA[c,e]	liquid	inter[a]	0	−140	0	2	7	20	−110	12.5
1,**2**-HA[c,e]	solid	inter[a]	0	−140	0	−3	7	20		
Intramolecular O2H2N2 Hydrogen Bond										
1,**2**,**3**-HA	liquid	intra[b]	0	−158	−5	4	6	20	−105	12.5
1,**2**,**3**-HA[e,f]	solid	intra[b]	0	−158	−5	3	5	20		

[a] The ^{15}N chemical shifts of the intermolecular O1H1N1 hydrogen bond are referenced to solid **1a**, resonating at 282.5 ppm (ref 42) with respect to external solid $^{15}NH_4Cl$. [b] The ^{15}N chemical shifts of the intramolecular O2H2N2 hydrogen bond are referenced to the methoxy-protected *N*-(2-methoxybenzylidene)-methylamine, resonating at 279.5 ppm (ref 40) with respect to solid $^{15}NH_4Cl$. [c] Ref 24. [d] Ref 68. [e] Ref 42. [f] Ref 40.

Thus, the interaction with the polar solvent has several effects. First, as was discussed previously for pyridine,[24,31−33,43] an increase in the acidity of the donor and of the solvent polarity shifts the proton continuously from oxygen to nitrogen, i.e., from O−H···N via $O^{\delta-}\cdot\cdot H\cdot\cdot N^{\delta+}$ to $O^-\cdot\cdot\cdot H-N^+$, where $O^{\delta-}\cdot\cdot H\cdot\cdot N^{\delta+}$ exhibits the shortest distance O···N. The shortest NH distance is achieved in methanol. Second, there is probably a distribution of hydrogen bond geometries that breaks down in the world of chemical shifts to a single averaged value.[32] This behavior is typical for a low-barrier hydrogen bond.

Metzler and co-workers reported for O1H1N1 in AspAT at pH 8.97 in aqueous solution a ^{1}H chemical shift of 15.39 ppm.[18−22] As illustrated in Figure 5a, this value is consistent with two possible ^{15}N chemical shifts of this hydrogen bond and hence two possible different hydrogen geometries, where the proton is either located closer to oxygen or closer to nitrogen. Thus, in order to characterize the hydrogen bond geometry further one needs additionally either the corresponding ^{15}N chemical shift or the scalar coupling constant to ^{15}N discussed below. Additionally, it is interesting to note that resonance Raman studies of Schiff base models show some evidence that the pyridine nitrogen can be protonated.[81−83] By contrast, the intramolecular OHN hydrogen bond behaves in a different way as illustrated in Figure 5b. Here, the ^{1}H chemical shifts do not follow the correlation line but are located on one of the upper straight dashed lines calculated using eq 13 for the case of a fast tautomeric equilibrium between two forms. An interesting observation is made. The data points are located either on the left or the right wings. Thus, either the OH- or the NH-form dominates. The data points on the left wing correspond to the free Schiff bases, whereas those on the right wing correspond to the acid−base complexes. Here, the doubly zwitterionic NH forms are stabilized by polar solvents, with methanol exhibiting the largest effect. The nondominating tautomers form stronger and shorter hydrogen bonds than the dominating forms. In other words the geometries of the OH and NH forms depend on whether the pyridine ring is involved in a hydrogen bond to an acid or not. This finding contrasts with the gas-phase result where unique hydrogen bond geometries for the OH and NH forms were obtained. Moreover, the predicted equilibrium averaged structures are away from those observed experimentally. We attribute this finding to the influence of the polar solvents.

Recently, it was proposed to use q_1 values and hence ^{15}N chemical shifts of acid−pyridine complexes as measures of the acidity of proton donors in nonaqueous environments.[42] Hence, it was not surprising that there was a reasonable correlation of the q_1 values with the corresponding pK_a values of the acids in water. The interested reader can find a plot of the pK_a value as a function of the ^{15}N chemical shifts measured here in Figure S10 of the Supporting Information.

^{1}H−^{15}N Coupling Constants. In Figure 6a, the one-bond scalar coupling constants ^1J(O1H1N1) of the Schiff bases and their adducts are plotted as a function of the corresponding ^{15}N chemical shifts. The data points are well located on the correlation curve predicted using eqs 5 and 7 as described in the Theoretical Section. A similar correlation was observed previously for pyridine derivatives−acid complexes.[24,32,33]

In Figure 6b the one-bond scalar coupling constants ^1J(O2H2N2) of the intramolecular hydrogen bonds of the Schiff bases and their adducts are plotted as a function of the ^{15}N chemical shifts. The solid line represents the hydrogen bond correlation curve, and the dashed line shows the equilibrium averaged values given by

$$\bar{J}(\mathrm{O\underline{HN}}) = \frac{J(\mathrm{O\underline{HN}})^{\mathrm{NH}} - J(\mathrm{O\underline{HN}})^{\mathrm{OH}}}{\delta(\mathrm{OH\underline{N}})^{\mathrm{NH}} - \delta(\mathrm{OH\underline{N}})^{\mathrm{OH}}}(\bar{\delta}(\mathrm{OH\underline{N}}) - \delta(\mathrm{OHN})^{\mathrm{OH}}) + J(\mathrm{OHN})^{\mathrm{OH}} \quad (14)$$

The difference between the two lines is barely pronounced. Therefore, coupling constants do not constitute a good diagnostic tool to distinguish low-barrier hydrogen bonds from those characterized by a tautomerism between two forms.[40] On the other hand, if a tautomeric equilibrium has been established from a ^{1}H/^{15}N chemical shift plot as illustrated in Figure 5b, such a plot helps to determine the intrinsic ^{15}N chemical shifts of the two forms from the intersections of the dashed lines with the correlation curves. Thus, the intrinsic ^{1}H−^{15}N coupling constants (Table 2) can be obtained from a plot such as that shown in

(81) Benecky, M. J.; Copeland, R. A.; Hays, T. R.; Lobenstine, E. W.; Rava, R. P.; Pascal, R. A., Jr.; Spiro, T. G. *J. Biol. Chem.* **1985**, *260*, 11663−11670.
(82) Benecky, M. J.; Copeland, R. A.; Rava, R. P.; Feldhaus, R.; Scott, R. D.; Metzler, C. M.; Metzler, D. E.; Spiro, T. G. *J. Biol. Chem.* **1985**, *260*, 11671−11678.
(83) Ledbetter, J. W. *J. Phys. Chem.* **1982**, *86*, 2449−2451.

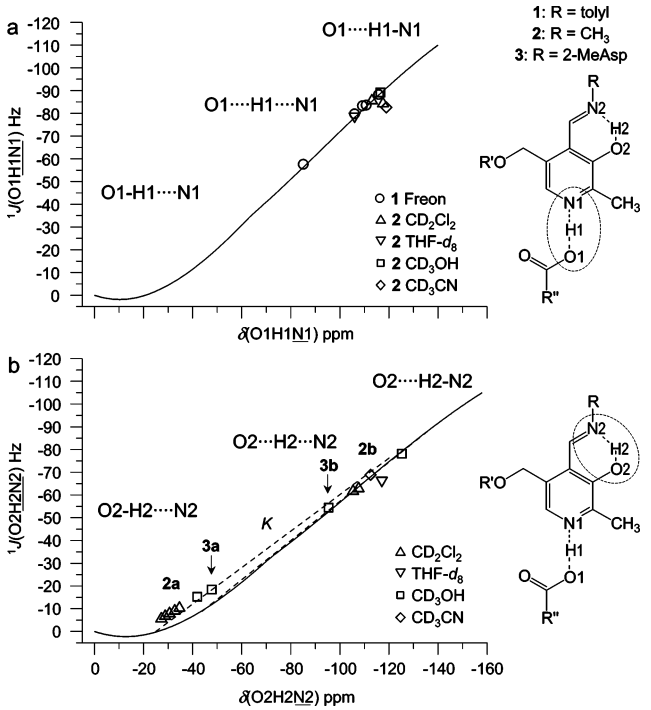

Figure 6. Scalar coupling constant ^1J(OHN) vs ^{15}N chemical shift δ(OHN) correlations: (a) shown for the intermolecular O1H1N1 hydrogen bond of **1** and **2**; (b) shown for the intramolecular O2H2N2 hydrogen bond of **2** and **3**. For further explanation, see text.

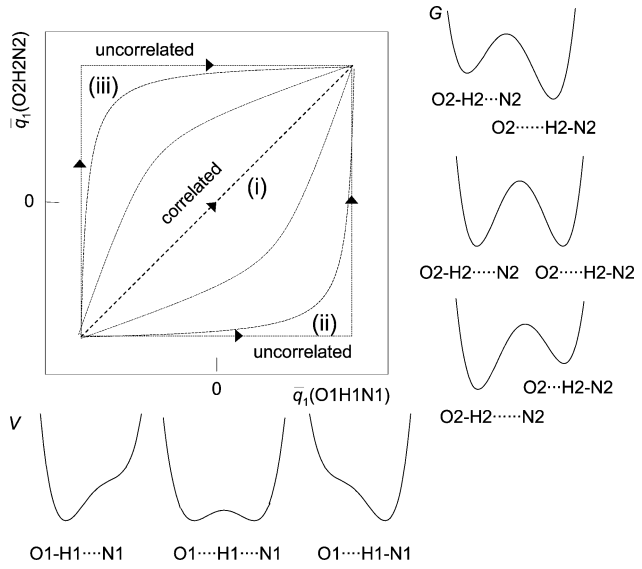

Figure 7. Visualization of the coupling of the inter- and the intramolecular OHN hydrogen bonds of internal and external aldimines in terms of average H-bond geometries. They indicate how the two average H-bond geometries may evolve in a series of stationary states, produced by changes of the structure or environments. In (i) the average geometries of both H-bonds are changed simultaneously; in (ii) the O1H1N1 bond is first changed from the initial to the final state, and then the O2H2N2 bond. In (iii) the contrary is realized. Intermediate correlation pathways are possible as indicated schematically.

Figure 6b. Finally, these limiting values allow one then to calculate the equilibrium constants K of tautomerism using eq 10, taking into account the influence of the solvent, the dielectric constant, microsolvation, etc.[40]

The logarithms of the equilibrium constants for tautomerism of O2H2N2 obtained in this way were plotted as a function of the inverse temperature from which averaged enthalpies (ΔH) and entropies (ΔS) of the tautomerism in Scheme 2 were obtained. As an example, we found for **2a** in CD_2Cl_2 values of $\Delta H = -6.1 \pm 0.4$ kJ mol^{-1} and $\Delta S = -47.4 \pm 2$ J K^{-1} mol^{-1}. In the case of the complex **2b**, the NH form was more populated as $\Delta H = -8.0 \pm 0.2$ kJ mol^{-1} and $\Delta S = -39.5 \pm 0.8$ J K^{-1} mol^{-1}.

In previous work it was shown that the three-bond vicinal coupling constants of aromatic Schiff bases and the values of the one-bond scalar coupling constants ^1J(O2H2N2) provide similar information.[40] It was shown also that both couplings depend linearly on each other, as expressed by eq 11. This equation was well satisfied in the case of **2**, as illustrated in Figure S11 in the Supporting Information.

Coupling of the Inter- and Intramolecular OHN Hydrogen Bonds. We come now to the question of the coupling of the low-barrier and medium-barrier OHN hydrogen bonds of the Schiff base−acid complexes in polar aprotic solvents. Several possibilities are depicted in Figure 7, where we plot the proton coordinate q_1 of O2H2N2 averaged over the OH/NH tautomerism according to eq 12 as a function of the proton coordinate q_1 of O1H1N1. Both coordinates are averaged over all solvents. The starting point is located at the lower left corner, and the end point is at the upper right corner, corresponding to limiting hydrogen bond geometries.

The proton motion in O1H1N1 occurs mostly in asymmetric single well potentials, besides the quasi-symmetric region where a low-barrier hydrogen bond may be realized as indicated schematically in Figure 7. By contrast, the proton motion in O2H2N2 always involves a barrier. The correlation curves in Figure 7 indicate how the two average H-bond geometries evolve in a series of stationary states, produced by changes of the structure or environments. Thus, each point on a correlation curve corresponds to a stable stationary point. In the "correlated" pathway (i) the average geometries of both H-bonds are changed simultaneously. Thus, when O1H1N1 forms a quasi-symmetric low-barrier hydrogen bond, the equilibrium constant of the OH/NH tautomerism in O2H2N2 is unity. As a substantial part of this equilibrium arises from a nonvanishing reaction entropy emerges solvent reorientation, the potential curve of the proton motion may still be asymmetric. The "uncorrelated" pathway (ii) corresponds to the case where the proton shift in O1H1N1 has no effect on the geometry of O2H2N2. Pathway (iii) is also of the uncorrelated type; here, O2H2N2 is first converted to the NH form and only later is O1H1N1 converted.

Since the ^{15}N chemical shifts of both hydrogen bonds are measures of the average proton bond coordinates $\bar{q}_1$, we plotted in Figure 8 the experimental ^{15}N chemical shifts of O2H2N2 of the Schiff base models **1** to **2** in different environments as a function of the ^{15}N chemical shifts of the corresponding O1H1N1 hydrogen bonds. The correlation lines are presented as guides for the eye. The recently observed data obtained for the solid state[42] and for aqueous solution[12] are included in the plot, which can be thought of as translations of the geometrical changes in the two hydrogen bonds. The lower left starting point and the upper right end point of the correlation lines correspond to specific hydrogen bond geometries and should not be confused with the limiting ends of the correlation curves in Figure 5.

For solid Schiff base **1** and its solid-state adducts we find that a proton shift in O1H1N1 has little effect on the average

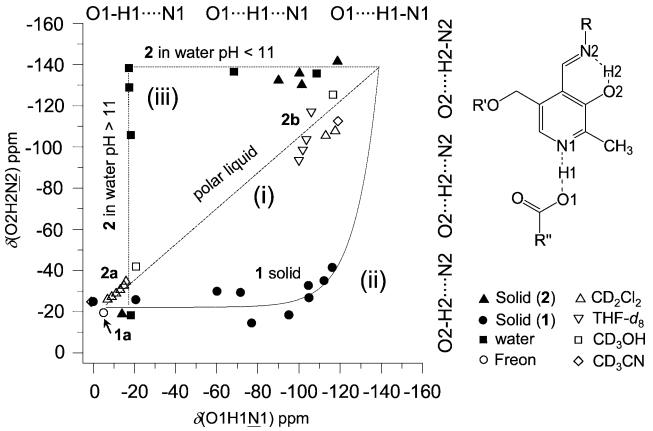

Figure 8. Plot of the δ(O2H2N2) vs δ(O1H1N1) chemical shift of **1** and **2** in different environments. The values of **1** and **2** in the organic solid state are obtained from ref 42. The values of **2** in aqueous solution are obtained from ref 12. For further explanation, see text.

geometries of O2H2N2 as expected for pathway (ii) in Figure 7. Here, evidence was obtained that the OH distances of O2H2N2 are only slightly increased and the HN distances slightly decreased without significant formation of an NH form. We associated this finding with the low basicity of the Schiff base nitrogen (which carried a tolyl substituent) (Scheme 4) as found previously for other Schiff bases.[41,42]

By contrast, the Schiff base **2a** carrying a methyl substituent and its adduct **2b** show a very different behavior. The data points of solid and of dissolved **2a** are located in the bottom left side of Figure 8. Small temperature, solvent, and solid−solvent-dependent shifts are observed which could arise either from hydrogen bond interactions with the OH side chain or other solid and solute−solvent interactions. The largest shift arises when methanol is used as a solvent.

The data points of the corresponding acid−base complexes appear in the upper right side of the graph. No intermediate data points were observed. This finding suggests that the basicities of the two nitrogen atoms in the polar environments are matched in such a way that a maximum coupling of the two hydrogen bonds is achieved (dashed straight line in Figure 8), representing the coupled pathway (i) in Figure 7. However, small deviations from this line are evident. The data of solid complexes **2b** O2H2N2 are located above and those for polar solution below the line. The limiting zwitterionic geometry of O2H2N2 is achieved for the solid **2a** already at lower degrees of conversion of O1H1N1 to the zwitterionic state as compared to polar aprotic solvents and to methanol.

On the other hand, the data points for Schiff base models in aqueous solution are not located on the above-mentioned curves. This indicates that the coupling between the two OHN hydrogen bonds is obliterated. When an ^{15}N chemical shift titration was performed, starting at low pH, both nitrogen atoms were protonated, i.e., data points are located in the upper right side of Figure 8. The horizontal shift of the data points to the left when the pH was increased reflects the deprotonation of the pyridine nitrogen. The chemical shift of the Schiff base nitrogen remains unchanged. Only around pH 10, when the pyridine ring is completely deprotonated does deprotonation of the Schiff base nitrogen occur, leading to a sudden drop of the data points of pathway (iii) on the left side of the graph.

The most probable reason for this decoupling is simply that the intramolecular hydrogen bond O2H2N2 is broken in aqueous solution into two separate functional groups, an imino function and a phenolic function which both exhibit different pK_a values, as was illustrated in Scheme 2d and as was postulated previously.[12]

The problem now arises whether the *decoupling* of the two hydrogen bonds in Schiff base adducts in aqueous solution arises from a bulk solvent dielectric effect or from specific interactions caused by a small number of proton donor groups. As discussed in the introduction and illustrated in Scheme 1, in the enzymic environment, the cofactor is involved in several specific hydrogen bonds from amino acid side chains in the active site. Is it conceivable that the intramolecular OHN hydrogen bond is broken?

In Figure 8, the data point of **2b** (Scheme 4) in methanol was taken from the spectra of Figure 2b. This point is on one hand well located on the dashed straight correlation line representing pathway (i) in Figure 7. On the other hand the data point is also located not far away from the corresponding data point of **2a** at low pH in aqueous solution. Thus, one could argue that the intramolecular O2H2N2 hydrogen bond could perhaps also be broken in methanol. However, this interpretation is not corroborated by the values of the one-bond coupling constants ^1J(O2H2N2) depicted in Figure 2 and Table 2. The changes of the values with temperature indicate different equilibrium constants of tautomerism of **2b** in methanol, i.e., the presence of an intact O2H2N2 hydrogen bond.

Influence of the Histidine Residue. We would have liked to observe experimentally ternary complexes of **2b** with an imidazole group as model for the interaction of the cofactor with an aspartate and a histidine residue as illustrated in Scheme 1. Unfortunately, we could not detect such complexes to date. In order to obtain some indications of what might be the outcome of such a study we performed ab initio calculations of model Schiff base adducts (Figure 3) at the HF level of theory. The ternary complex **2d**(OH,NH) shows only a small energy difference in comparison with the imidazole-lacking **2c**(OH,-NH). In contrast, **2d**(NH,NH) is significantly favored when the proton in the intermolecular OHN hydrogen bond is transferred to the pyridine nitrogen; therefore, the imidazole moiety stabilizes the zwitterionic structure. This finding is in agreement with recent NMR studies which show that an additional proton donor can shift a proton in a OHN hydrogen bond toward the nitrogen,[30,33,84] which was also demonstrated for the 2:1 acid−base complex **1j** (Figure 1) where the proton-donating power of the linear acid dimer is larger than that of the monomer in the corresponding 1:1 complex of **1g**.

Conclusions

Using NMR spectroscopy of suitably ^{15}N-labeled compounds, we have demonstrated that the functional OHN hydrogen bonds of Schiff base cofactor models **1**−**3** embedded in polar solvents can be characterized by a combination of ^{1}H and ^{15}N NMR spectroscopy using hydrogen bond correlation techniques. The intermolecular OHN bonds to the pyridine ring (Scheme 1) are best characterized as low-barrier hydrogen bonds, yielding a

(84) Rospenk, M.; Sobczyk, L.; Schah-Mohammedi, P.; Limbach, H. H.; Golubev, N. S.; Melikova, S. M. *Magn. Reson. Chem.* **2001**, *39*, S81−S90.

maximal shortening of the O···N distance when the quasi-symmetric hydrogen bond $O^{\delta-}\cdot\cdot H\cdot\cdot N^{\delta+}$ is formed. By contrast, a classical tautomerism is found for the intramolecular OHN hydrogen bonds. When the Schiff base nitrogen carries an aliphatic substituent (as found in the internal or external aldimines of PLP in enzyme active sites) (Scheme 1) the basicity of the two nitrogen atoms are relatively matched, leading to a cooperative coupling of the two hydrogen bonds. This coupling is such that a quasi-symmetric intermolecular OHN hydrogen bond implies an equilibrium constant of approximately unity for the tautomerism in the intramolecular OHN hydrogen bond. The latter is broken in water, but not in methanol. As the presence of the intramolecular OHN hydrogen bond appears to be essential for enzyme activity, it follows that polar aprotic solvents provide more suitable environments to model the cofactor embedded in the active site of enzymes than does aqueous solution. Biochemically, these results have the important implications that differential protonation of the pyridine ring of the coenzyme in active sites can modulate reactivity and reaction specificity by modulating the electron-withdrawing ability of the pyridine ring and the protonation state of the Schiff base nitrogen.

Acknowledgment. This work was supported by the Deutsche Forschungsgemeinschaft, Bonn, and the Fonds der Chemischen Industrie, Frankfurt.

Supporting Information Available: Complete set of NMR spectra of **1** dissolved in $CDF_3/CDClF_2$ and of **2** in a variety of different organic solvents, in particular, acetonitrile-d_3, methanol-d_3, tetrahydrofuran-d_8, and $CDF_3/CDClF_2$; low-temperature spectra of the amino acid−substrate **3** dissolved in CD_3OH; selected geometrical parameters of the optimized structures calculated at the HF level of theory; complete ref 59. This material is available free of charge via the Internet at http://pubs.acs.org.

JA070296+